Mon. Not. R. Astron. Soc. **000**, 1–19 (2009) Printed 7 September 2009 (MN LATEX style file v2.2)

# 2MASS photometry of edge-on spiral galaxies. I. Sample and general results

A. V. Mosenkov, N. Ya. Sotnikova⋆ and V. P. Reshetnikov
*St.Petersburg State University, Universitetskij pr. 28, 198504 St.Petersburg, Stary Peterhof, Russia*
*and Isaac Newton Institute of Chile, St.Petersburg Branch*



Accepted 2009 September 6. Received September 6; in original form 2009 July 2

**ABSTRACT**

A sample of edge-on spiral galaxies aimed at a thorough study of the main structural and photometric parameters of edge-on galaxies both of early and late types is presented. The data were taken from the Two Micron All Sky Survey (2MASS) in the $J$, $H$ and $K_s$ filters. The sources were selected according to their angular size mainly on the basis of the 2MASS-selected Flat Galaxy Catalog (2MFGC). The sample consists of 175 galaxies in the $K_s$-filter, 169 galaxies in the $H$-filter and 165 galaxies in the $J$-filter. We present bulge and disc decompositions of each galaxy image. All galaxies have been modelled with a Sérsic bulge and exponential disc with the BUDDA v2.1 package. Bulge and disc sizes, profile shapes, surface brightnesses are provided.

Our sample is the biggest up-to-date sample of edge-on galaxies with derived structural parameters for discs and bulges. In this paper we present the general results of the study of this sample. We determine several scaling relations for bulges and discs which indicate a tight link between their formation and evolution. We show that galaxies with bulges fitted by the Sérsic index $n \lesssim 2$ have quite different distributions of their structural parameters than galaxies with $n \gtrsim 2$ bulges. At a first approximation the Sérsic index threshold $n \simeq 2$ can be used to identify pseudobulges and classical bulges. Thus, the difference in parameter distributions and scaling relations for these subsamples suggests that two or more processes are responsible for disk galaxy formation. The main conclusions of our general statistical analysis of the sample are:

(1) The distribution of the apparent bulge axis ratio $q_{\rm b}$ for the subsample with $n \lesssim 2$ can be attributed to triaxial, nearly prolate bulges that are seen from different projections, while $n \gtrsim 2$ bulges seem to be oblate spheroids with moderate flattening. Triaxiality of late-type bulges may be due to the presence of a bar that thickened in the vertical direction during its secular evolution.

(2) For the sample galaxies, the effective radius of the bulge $r_{\rm e,b}$, the disc scalelength $h$ and the disc scaleheight $z_0$ are well correlated. However, there is a clear trend for the ratio $r_{\rm e,b}/h$ to increase with $n$. As $n$ is an indicator of the Hubble type, such a trend unambiguously rules out the widely discussed hypothesis of a scale-free Hubble sequence. The found correlation between $z_0$ and $r_{\rm e,b}$ is new and was not described earlier.

(3) There is a hint that the fundamental planes of discs, which links only disc parameters and the maximum rotational velocity of gas, are different for galaxies with different bulges. This may indicate a real difference of discs in galaxies with low and high concentration bulges.

(4) The most surprising result arises from the investigation of the Photometric Plane of sample bulges. It turns that the plane is not flat and has a prominent curvature towards small values of $n$. For bulges this fact was not noticed earlier.

(5) The clear relation between the flattening of stellar discs $h/z_0$ and the relative mass of a spherical component, including a dark halo, is confirmed not for bulgeless galaxies but for galaxies with massive bulges.

Many of our results are in good agreement with the results of other authors, several ones are new. Thus, our sample is very useful for further detailed studying and modelling of the edge-on spiral galaxies.

**Key words:** galaxies: fundamental parameters — galaxies: general — galaxies: infrared — galaxies: spiral edge-on galaxies — galaxies: photometry.

## 1 INTRODUCTION

The photometric and kinematic study of spiral galaxies provides a method to tackle the problems concerning their formation and evolution. A lot of observational data has been obtained in recent decades, especially with the advent of CCD arrays. Over the last years, significant progress has been made in both observational and theoretical studies aimed at understanding the structure and evolution of galaxies. Modern sky surveys (2MASS, SDSS, etc.) provide information on the characteristics and spatial distribution of millions of galaxies. The large available amount of information has altered the face of modern extragalactic astronomy. Many important tasks, including detailed photometric studies of the structure of nearby galaxies, can be now solved without additional observations by telescopes. Here we focus on the surface photometry of spiral galaxies on the basis of the 2MASS near-infrared survey.

The parametrization of galaxies is a way to describe the multitude of normal galaxies without any peculiarities within their structure. Various fitting functions are used to derive structural parameters of bulges and discs. Traditional fitting functions for stellar discs include an exponential function (de Vaucouleurs 1959, Freeman 1970) and an inner-truncated exponential function (Kormendy 1977). Bulges are well described by the so-called Sérsic profile that includes the de Vaucouleurs profile as a special case (Sérsic 1968). The de Vaucouleurs law, or $r^{1/4}$-law, was obtained empirically for elliptical galaxies (de Vaucouleurs 1948) and later for bulges of early-type galaxies (de Vaucouleurs 1959). Later it was shown that the Sérsic law is preferable to fit spheroidal components of galaxies (e.g. Andredakis et al. 1995). The $z$-distribution of surface brightness of edge-on discs is exponential or the so called "sech$^2$-distribution" (van der Kruit & Searle 1981). (All the mentioned functions are described in Section 3 of this paper.)

In order to derive structural parameters of bulges and discs, we must perform photometric bulge/disc decomposition of galaxy images. There are numerous methods of such decomposition. The one-dimensional analysis of the surface-brightness distribution is the most commonly used method (e.g. Boroson 1981; Kent 1985; Baggett, Baggett & Anderson 1998; Bizyaev & Mitronova 2002, hereafter BM02). But as was shown by Byun & Freeman (1995) the one-dimensional decomposition procedure leads to strong systematic errors. The two-dimensional approach provides much better estimates of the structural parameters for each component of a galaxy. This method is powerful when we need to separate the non-axisymmetric structures (bars, rings, spiral arms) from axisymmetric components (disc and bulge).

In recent decades a number of studies concerning structural properties of galaxies has been performed. The results of decompositions of near face-on disc dominated galaxies as well as of early-type galaxies were presented, for instance, by de Jong (1996). It was concluded that there is a correlation between structural parameters of discs and bulges. Möllenhoff & Heidt (2001) found similar correlations and speculated about the formation and evolution of spiral galaxies. Graham (2001) performed a detailed analysis of low-inclination spiral galaxies and described many significant properties of their bulges and discs. Other studies dealt with the correlation between the scalelengths of bulges and discs (e.g. Courteau et al. 1996; de Jong 1996), the presence of additional morphological components such as bars, lenses, rings, inner bars and inner discs (e.g. de Souza, Gadotti & dos Anjos 2004, SGA04 hereafter; Castro-Rodríguez & Garzón 2003; Laurikainen, Salo & Buta 2005; Gadotti 2009) and the revision of morphological classification of galaxies (SGA04). The fundamental plane (FP) of discs as well as the photometric plane of bulges were also widely discussed (e.g. Khosroshahi et al. 2000a,b; Möllenhoff & Heidt 2001; Moriondo, Giovanelli & Haynes 1999).

The main aim of our project is to perform decompositions of a large number of edge-on galaxies both of early and late types into bulges and discs. We chose this type of galaxies because they provide a unique possibility to obtain information about the vertical structure of galactic discs. In the edge-on view non-axisymmetric features such as bars, rings or spiral arms are not seen. On the other hand, the vertical distribution of light in edge-on galaxies allows us to study a thin disc, a thick disc and a stellar halo (see e.g. Yoachim & Dalcanton 2005; Seth, Dalcanton & de Jong 2005).

Unfortunately, there are some difficulties in studying edge-on galaxies. In the optical band we need to take into account the dust extinction in the plane of a disc. The distribution of dust is often unknown and it is hard to obtain true values of disc and bulge parameters. The advantage of NIR observations is that the general extinction is drastically reduced, although we can not exclude it completely. Nevertheless it is better to perform the decomposition of galaxies by using their images in red and infrared bands. Using three IR bands for galaxy decomposition and subsequent statistical analysis of galaxy properties in all three bands encourages us in our suggestion that extinction problems are not very severe (at least for general statistical correlations which are the subject of the present work). However, edge-on galaxies are rare in occurrence in contrast to face-on galaxies or galaxies with intermediate inclination angles. Therefore, in order to create a large sample of edge-on galaxies it is necessary to use special catalogues which include a lot of edge-on spiral galaxies such as the Revised Flat Galaxy Catalog (Karachentsev et al. 1999).

A detailed study of the disks of edge-on galaxies is described in many papers (e.g., van der Kruit & Searle 1981; Reshetnikov & Combes 1997; de Grijs 1998). In a more recent study, Dalcanton & Bernstein (2000, 2002) examined a sample of extremely late-type, edge-on spirals with no apparent bulges and concluded that thick disks are common around galaxy disks of all masses. BM02 also analyzed a sample of late-type edge-on galaxies in the $J$, $H$ and $K_s$-bands to compare the mean ratios $h/z_0$ in these bands. They have noted a strong correlation between the central surface brightness of the disk and the $h/z_0$ ratio: the thinner the galaxy, the lower the central surface brightness reduced to the face-on inclination. Kregel, van der Kruit & de Grijs (2002), Kregel (2003), Kregel, van der Kruit & Freeman (2005) and Zasov et al. (2002) presented a complex study (dynamical properties of the stellar discs, three-dimensional disc structure, stellar kinematics, rotation curves) of several dozens of edge-on spirals. Unfortunately, there are no extended studies of structural parameters of edge-on galaxies both of early and late types which join analysis of their

bulges and discs. Our study is intended to fill this gap. We analyse the statistical properties of the sample edge-on galaxies and present correlations between the global structural parameters of *bulges* and *discs*, including those that describe their vertical structure, in the near-infrared bands.

This paper is organized as follows. In Section 2 we present the detailed description of our sample of spiral edge-on galaxies which includes the selection criteria and a brief description of the data sources. We also describe the completeness of the sample and its main properties. In Section 3 we use the two-dimensional least-squares algorithm to decompose the galaxy images into a bulge and a disc. We recall some aspects of the code BUDDA (SGA04) which we used as the decomposition tool. In Section 4, we present the results of image decomposition in the $J$, $H$ and $K_s$-bands. We compare our results with previous results from the literature and analyse the reliability of the results of the BUDDA decompositions. In Section 5 we describe general properties of edge-on spiral galaxies and discuss some correlations between galactic subsystems. Some of them are well-known but there are also some new results. In Section 6 we summarize our main conclusions. In the forthcoming papers we are going to discuss properties of edge-on galaxies in more detail.

## 2 THE SAMPLE

We intended to find edge-on galaxies with a wide range of bulges: from bulge-dominated spirals to galaxies with small bulges. We used the 2MASS-selected Flat Galaxy Catalog (2MFGC) (Mitronova et al. 2003) as a source of objects and the 2MASS survey (Skrutskie et al. 2006) as a source of image data. We also used the Revised Flat Galaxies Catalog (RFGC) by Karachentsev et al. (1999) to add late-type galaxies to our sample.

The Two Micron All Sky Survey is one of the best known digital surveys in a wavelength range close to the optical one. This survey covers the whole sky in the filters $J$ (1.25 $\mu$m), $H$ (1.65 $\mu$m), and $K_s$ (2.16 $\mu$m). Unfortunately, the 2MASS survey has a weak sensitivity to late-type galaxies, especially of low surface brightness (Jarrett 2000). This is due to the high brightness of the night sky in the near-IR range and short exposures. For this reason the periphery of the discs of spiral galaxies is generally unseen beyond the isophotes fainter than $\mu_K = 20$ mag arcsec$^{-2}$. We did not study truncation radii for the 2MASS-galaxies and did not take them into account performing the decomposition.

The sample was selected mainly from the 2MFGC. This catalogue contains 18020 disc-like galaxies covering all the celestial sphere. The objects were taken from the Extended Source Catalog of the 2MASS (XSC 2MASS) according to their 2MASS axial ratio $a/b \geqslant 3$. The 2MFGC gives value of axial ratio $b/a$, fiducial elliptical Kron magnitude, position angle, the $J$-band concentration index ($IC$) and other useful information. Concentration index is the ratio of the radii of circles that contain 3/4 and 1/4 of the measured flux in the same band, respectively. $IC$ together with $b/a$ are known to serve as dividing lines between early- and late-type galaxies (see e.g. Strateva et al. 2001; Nakamura et al. 2003). We decided to select galaxies both of early and late types in almost equal quantities. Our criteria are

- axial ratio for the combined $J+H+K$ image, $sba > 0.2$;
- $K$-band fiducial elliptical Kron radius, $R_K \geqslant 30''$;
- Hubble type ranging from S0 to late types;
- non-interacting galaxies;
- concentration index $IC > 2.0$.

The latter item means that we exclude galaxies with strongly peculiar surface brightness distributions since for pure exponential disks $IC = 2.8$ and for $r^{1/4}$ ellipticals $IC = 7$ (Fraser 1972).

From the set of 3167 objects which contains galaxies with pronounced bulges (Sa, Sb types) and galaxies with small bulges (Sc, Scd types) we selected a sufficient number of regular spiral galaxies to make statistical analysis of edge-on galaxies properties. We did not add to the sample galaxies that are clearly lopsided or warped (with some exceptions below). In addition, on the basis of careful visual inspection we rejected non-edge-on and peculiar objects. Also, we added 13 bright galaxies that were absent in the 2MFGC and several edge-on galaxies which were not selected according with foregoing criteria but were included in the sample of RFGC galaxies by BM02. We chose them to compare the results of our decomposition with those obtained by BM02.

The final sample consists of 67 early-type galaxies (S0-Sab), 61 late-type galaxies (Sbc-Sd) and 47 galaxies of intermediate type Sb. The absolute numbers of galaxies of various morphological types (taken from the LEDA) and their percentages are listed in the Table 1. The full list of the sample galaxies studied here is presented in the Appendix, where we provide the basic information about them. According to LEDA 23 galaxies have bars, 6 galaxies have rings, and 3 objects are interacting galaxies. We did not take into account additional components like bars performing the decomposition, but checking all correlations between structural parameters, we did not find any strong deviation of the above-mentioned objects from derived trends.

We also did not reject 3 interacting galaxies and several other galaxies with some unusual structural features (double exponential discs, rings, etc., which will be described in our resulting tables) to have about 10 unusual spiral edge-on galaxies for further work.

As can be seen in the Table 1 the sample contains a substantial percentage of lenticular galaxies. It is necessary to notice that Hubble classification for edge-on galaxies is very subjective because the spiral arm structure is not seen in this case. The only way to classify edge-on galaxies according to morphological types is the estimation of the ratio of the total luminosities of a bulge and a disc (hereafter $B/D$). We assume that a large fraction of classified S0 galaxies are Sa galaxies in fact. In Fig. 1 the images of typical sample galaxies are shown. According to the LEDA data, our sample galaxies are, on average, true highly-inclined galaxies with the mean inclination $i = 87.^\circ8 \pm 4.^\circ8$. Of course, this estimate can be too optimistic but a moderate deviation from edge-on orientation does not significantly change the slope of the vertical surface brightness distribution (Barteldrees & Dettmar 1994).

The distances of the galaxies are taken from NASA/IPAC Extragalactic Database (NED) with the Hubble constant $H_0 = 73$ km s$^{-1}$/Mpc, $\Omega_{\rm matter} = 0.27$, and $\Omega_{\rm vacuum} = 0.73$). The luminosity distances are in the range from 4.3 Mpc (NGC 891) to 171 Mpc (ESO 251-G028) with

**Table 1.** Morphological types of the sample galaxies and their fractions

| Type | Number | Percentages |
|---|---|---|
| S0, S0-a | 41 | 23.4 |
| Sa | 11 | 6.3 |
| Sab | 15 | 8.6 |
| Sb | 47 | 26.9 |
| Sbc | 21 | 12.0 |
| Sc | 36 | 20.5 |
| Scd | 4 | 2.3 |
| Total | 175 | 100 |

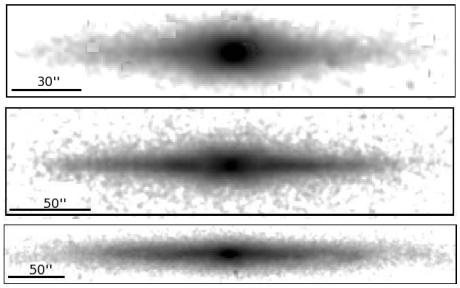


**Figure 1.** Examples of the sample galaxies in the $K_s$-band. The upper image is a typical galaxy of S0-a type: ES0 311-G012. The middle image is NGC 4013 of Sb type. The bottom image is an example of Sc galaxy: NGC 5907.

a sample median value of 40 Mpc. Three galaxies (ESO 013-G024, ESO 555-G023, ESO 555-G032) have no measured or estimated distances. We do not take them into account in statistical analysis where the distances are required.

To investigate some kinematical and dynamical properties of the sample galaxies we added information about maximum rotation velocity for each galaxy if it was presented in the LEDA data base (see the section 5.3 for more details).

The sample consists of 175 galaxies in the $K_s$-filter, 169 galaxies in the $H$-filter and 165 galaxies in the $J$-filter. (Several galaxies have prominent dust lanes within their discs and even in the $J$ and $H$ passbands absorption of the dust is significant.)

In order to evaluate the completeness of the sample, we use the method proposed by Schmidt (1968) (the so-called $V/V_{\rm max}$ completness test). Following Thuan & Seitzer (1979) we used this method for our angular-size-limited sample. The full sample is incomplete but the subsample of galaxies with angular radius $r \geqslant 60''$ is complete ($V/V_{\rm max} = 0.49 \pm 0.03$). This subsample consists of 92 galaxies (47 early-type galaxies and 45 late-type galaxies).

The images used in this work were taken from the database of the All-Sky Release Survey Atlas. The Atlas' images are FITS standard images in 512 × 1024 pixel format (with $1.''00$ pixel$^{-1}$). Description of the images such as the pixel gain, readout noise, seeing FWHM ($\sim 2.''5$), sky value and also zero points are available in the 2MASS webpages. This information has been used in making decompositions of galaxy images. Each image was thoroughly examined in order to mask background stars and galaxies and other contaminating sources. All the images were rotated to align the galaxy major axis parallel to the horizontal image borders. These procedures were carried out in three filters so all images of the same galaxy in the $J$, $H$ and $K_s$ bands have the same extension and position angles. The smallest image of our sample is 48×18 pixels for ESO 555-G032 and the largest image is 869×165 pixels for NGC 4565. The median value of the size of galaxy images is 119×27 pixels, that is enough to determine the main photometric parameters of galaxy discs and bulges. The forthcoming analysis was performed with the MIDAS (developed by the European Southern Observatory) and the BUDDA packages.

## 3 TWO-DIMENSIONAL BULGE/DISC DECOMPOSITION

BUDDA (Bulge/Disc Decomposition Analysis) is a code devised to perform two-dimensional decomposition of galactic images. This code was produced by R.E. de Souza, D.A. Gadotti and S. dos Anjos (for more information about BUDDA see SGA04). Since the year of 2004 BUDDA has been publicly available to the astronomical community[1]. We use BUDDA v2.1 to produce the fits, allowing the inclusion of bulges, discs, bars and AGN in the models.

The input data for the code is an image of a galaxy, consisting of two major components: a bulge and a disc. The disc is represented by an exponential distribution of the luminosity density $I(r, z)$ with the central luminosity density $I(0, 0)$, the scalelength $h$ and the 'isothermal' scaleheight $z_0$:

$$I(r, z) = I(0, 0)\, e^{-r/h}\, \mathrm{sech}^2(z/z_0)\,, \qquad (1)$$

where $(r, z)$ are the cylindrical coordinates. The disc is assumed to be axisymmetric and transparent.

The surface brightness distribution for the face-on disk ($i = 0^\circ$) can be expressed as follows:

$$I_{\rm d}(r) = I_{0,\rm d}\, e^{-r/h}, \qquad (2)$$

where $I_0 = 2\, z_0\, I(0, 0)$. The same expression in magnitudes per arcsec$^2$ is:

$$\mu_{\rm d}(r) = S_{0,\rm d} + 1.086\, r/h, \qquad (3)$$

where $S_{0,\rm d}$ is the central surface brightness of the face-on disc. For edge-on galaxies ($i = 90^\circ$) the following expression is valid:

$$I(r, z) = I(0, 0)\, \frac{r}{h}\, K_1\left(\frac{r}{h}\right)\, \mathrm{sech}^2(z/z_0)\,, \qquad (4)$$

where $K_1$ is the modified Bessel function of the first order.

The bulge surface brightness profile is described by the Sérsic law (Sérsic 1968):

$$I_{\rm b}(r) = I_{0,\rm b}\, e^{-\nu_{\rm n}[(r/r_{\rm e,b})^{1/n}]}\,, \qquad (5)$$

where $r_{\rm e,b}$ is the effective radius of the bulge, i.e., the radius of a circle that contains 50% of the total galaxy luminosity, $I_{0,\rm b}$ is the bulge central surface brightness, $n$ is the Sérsic index, defining the shape of the profile, and the parameter $\nu_n$ ensures that $r_{\rm e,b}$ is the half-light radius. In magnitudes per arcsec$^2$ the expression looks as follows:

$$\mu_{\rm b}(r) = \mu_{0,\rm b} + \frac{2.5\nu_{\rm n}}{\ln 10}\, \left(\frac{r}{r_{\rm e,b}}\right)^{1/n}\,, \qquad (6)$$

[1] see http://www.mpa-garching.mpg.de/∼dimitri/budda.html

where $\mu_{0,\mathrm{b}}$ is the bulge effective surface brightness expressed in mag per arcsec$^2$, i.e., the surface brightness at $r_{\mathrm{e,b}}$. The BUDDA code uses a numerical approximation of $\nu_n \simeq (0.868n - 0.142)\,\ln 10$. The Sérsic index of $n = 4$ represents the de Vaucouleurs profile which was very popular to describe the surface brightness distribution of bright elliptical galaxies and of bulges in early-type spirals. The Sérsic index of $n = 1$ represents the exponential profile of bulges in late-type spirals, of galactic discs and of dwarf elliptical galaxies (see e.g. de Vaucouleurs 1948, 1959; Freeman 1970; Graham 2001 and references therein).

It is also useful to determine such parameters as ellipticities ($\epsilon = 1 - b/a$) of a bulge $\epsilon_{\mathrm{b}}$ and a disc $\epsilon_{\mathrm{d}}$, as well as their position angles $P.A._{\mathrm{b}}$ and $P.A._{\mathrm{d}}$. To account for the effect of seeing there is a Moffat smearing (Moffat 1969) of the brightness profiles in the code controlled by a parameter associated with the seeing radius $a_{\mathrm{s}}$. There is also included a correction term of the sky level $\Delta_{\mathrm{sky}}$. The isophotes of bulges and discs can be described by generalized ellipses with the ellipse index parameter $\gamma$ controlling their shape:

$$\left(\frac{|x|}{a}\right)^{\gamma+1} + \left(\frac{|y|}{b}\right)^{\gamma+1} = 1, \qquad (7)$$

where $x$ and $y$ are the pixel coordinates of the ellipse points, $b$ and $a$ are the sizes of its semi-major and semi-minor axes, respectively. When $\gamma = 1$ the ellipse is simple, while for $\gamma > 1$ the ellipse is boxy and for $\gamma < 1$ the ellipse is discy.

For edge-on galaxies BUDDA derives the disc scaleheight $z_0$ instead of the disc ellipticity $\epsilon_{\mathrm{d}}$. Thus, a total number of the main parameters for the bulge/disc model is 11: the center coordinates $x_0$ and $y_0$, the central surface brightnesses of a bulge $I_{0,\mathrm{b}}$ (or the effective surface brightness of bulge $I_{\mathrm{e,b}}$ as used in BUDDA) and a disc $I_{0,\mathrm{d}}$ (both in ADU), $r_{\mathrm{e,b}}$, $h$, $P.A._{\mathrm{b}}$, $P.A._{\mathrm{d}}$, the disc scaleheight $z_0$, the bulge ellipticity $\epsilon_{\mathrm{b}}$ and the Sérsic index of a bulge $n$.

Total luminosity of a disc can be expressed as:

$$L_{\mathrm{D}} = 2\pi\, I_{0,\mathrm{d}}\, h^2\,, \qquad (8)$$

while the total luminosity of a bulge is

$$L_{\mathrm{B}} = \frac{2\pi n}{\nu_{\mathrm{n}}^{2n}}\,\Gamma(2n)\, I_{0,\mathrm{b}}\, r_{\mathrm{e,b}}^2\,(1-\epsilon_{\mathrm{b}})\,, \qquad (9)$$

where $\Gamma$ means the gamma function.

The code BUDDA allows the user to add some additional components in a galaxy model (bars, AGNs and double exponential discs), but we made decompositions of all our galaxies into a bulge and a disc only. There are some difficulties to determine the presence of a bar or any other substructures in edge-on perspective. The observed surface brightness distribution is a result of luminosity integration along the line of sight and such integration can smooth and hide such subcomponents. It is also hard to make the first approximation of the values of parameters which characterize these additional features.

Fig. 2 illustrates typical results of our decomposition for the Sb-type galaxy ESO 240-G011. The size of the image is 228×40 pixels. The sky background, Galactic stars, bright HII regions and nearby companions were removed. The derived parameters are given in Table 2. As seen in Fig. 2 the fit is fairly good.

**Table 2.** Parameters of the two-component model for ES0 240-G011 ($K_s$ band)

| | | | |
|---|---|---|---|
| $D$ (Mpc) | 35.7 | $\mu_{\mathrm{e,b}}$ | $17.09 \pm 0.09$ |
| | | $r_{\mathrm{e,b}}$ (kpc) | $1.34 \pm 0.09$ |
| $\mu_{0,\mathrm{d}}$ | $16.22 \pm 0.16$ | $n$ | $2.4 \pm 0.3$ |
| $h$ (kpc) | $5.1 \pm 0.9$ | $q_{\mathrm{b}}$ | $0.69 \pm 0.04$ |
| $z_0$ (kpc) | $0.80 \pm 0.13$ | $B/D$ | 0.38 |
| $h/z_0$ | 6.4 | $v_{\mathrm{rot}}$ (km/s) | $267.5 \pm 3.3$ |

## 4 DECOMPOSITION AND RESULTS

To start the galaxy decomposition, we must determine the first-order approximations for the input parameters (see previous section). To obtain the first-order approximation for our 2D fits, we have used parameters derived from 1D fits of the major and minor axes profiles.

In almost all cases the ellipse index $\gamma$ of a bulge was taken to be equal $1.0 \pm 0.01$ (for simplicity we consider bulges with elliptical isophotes). A galaxy with complex morphology of a bulge requires more detailed investigation with higher resolution images than those that are given by 2MASS. The result of decompositions into a bulge and a disc is the list of all structural parameters of each object of the sample in 3 photometric bands. The final values of $\mu_{\mathrm{e,b}}$ and $\mu_{0,\mathrm{d}}$ were corrected for the Galactic extinction according to Schlegel, Finkbeiner & Davis (1998).

To check the reliability of our 2D decompositions, we subtracted the full apparent magnitudes of our models from the apparent magnitudes presented in the 2MASS catalogue. The mean values and standard deviations of these subtractions for the sample galaxies are: $\Delta J = 0.^m011 \pm 0.^m057$, $\Delta H = 0.^m021 \pm 0.^m049$, $\Delta K_s = 0.^m014 \pm 0.^m053$.

Our sample has 30 galaxies in common with the sample of BM02. The method used by these authors is based on several photometric cuts parallel to the minor axis of each galaxy and parallel to its major axis. Their sample includes flat galaxies mainly of late types in the $K_s$ filter. Fig. 3 shows a comparison of radial scalelengths (the upper frame), vertical scale heights (the middle frame) and deprojected central surface brightness of discs (the bottom frame). Open squares are related to the objects which have some peculiarities or features in structure (NGC 5965, UGC 6012, UGC 12533 are with possible bars, IC 4202, UGC 4517, ESO 121-G006 are with strong dust lanes, and UGC 1817 is a bulgeless galaxy in a group). These objects do not lie on the diagonal. The mean values and standard deviations of difference between parameters obtained by us and by BM02 are:

$$\langle h - h_{\mathrm{BM}} \rangle = 2.''46 \pm 2.''11\,,$$

$$\langle z_0 - z_{0,\mathrm{BM}} \rangle = 0.''41 \pm 0.''29\,,$$

$$\langle S_0 - S_{0,\mathrm{BM}} \rangle = 0.^m28 \pm 0.^m19\,.$$

As one can see (Fig. 3), our results and those of BM02 are in good agreement.

De Grijs (1998) presented detailed surface photometry for a sample of edge-on galaxies in the $B$, $I$ and $K$ bands. Fig. 4 shows a comparison of radial scalelengths for 14 joint galaxies ($K$-band). Some systematics are evident which can be attributed to different decomposition procedures.

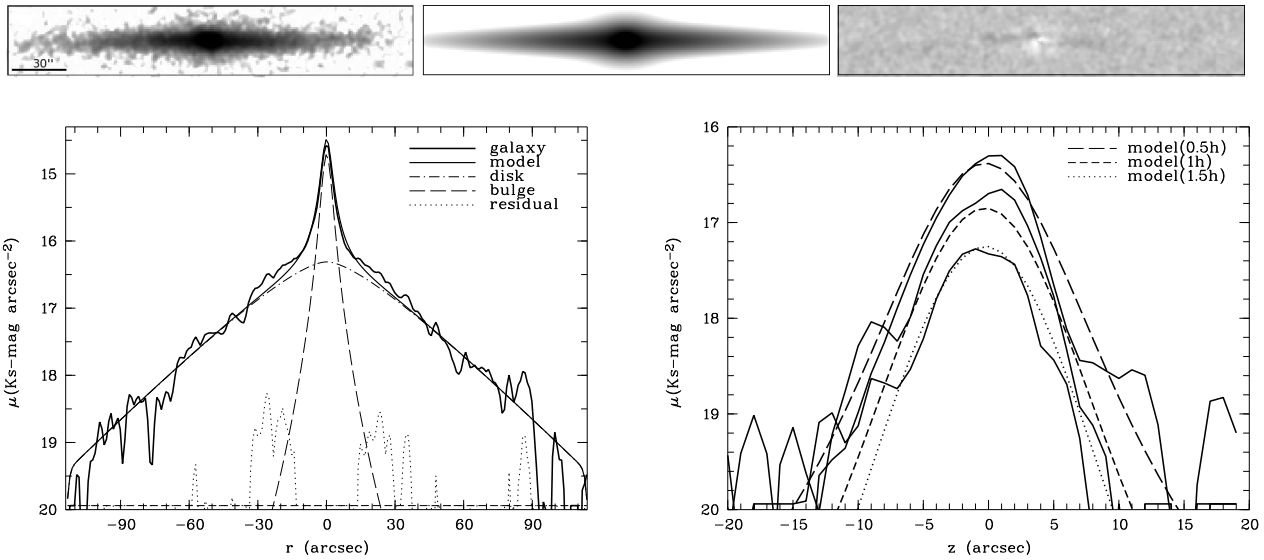


**Figure 2.** An example of the edge-on spiral galaxy ESO 240-G011 in the $K_s$-band. The images on the top show the galaxy (top left), the model (top middle) and the residual image (top right). The residua were obtained after subtraction of the model from the image. The bottom panels show the surface brightness profiles of the galaxy, the model and the residual images are indicated. The profiles are drawn along major- (left) and minor axes (right) at $r = 0.5h$, $1.0h$ and $1.5h$.

Table 3 compares decomposition results for 5 galaxies in the present work and in the paper by Bedregal, Aragon-Salamanca & Merrifield (2006). As one can see, the results are in agreement that is typical for such a comparison[2]. It proves the reliability of the obtained results and makes them suitable in our further statistical analysis.

## 5 MAIN RESULTS

Statistical correlations between structural parameters give us a clue for understanding the formation and evolution of spiral galaxies. Here we present only some of the correlations of the main parameters of the galaxies. The detailed analysis of the properties of bulges and discs will be done in a forthcoming article.

### 5.1 Distributions of structural parameters

Here we briefly describe the distributions of structural parameters of stellar components. In general, we do not take into account any corrections for the incompleteness and selection effects of the sample but in special cases we give the best fitting parameters obtained for the complete subsample.

#### *5.1.1 Discs*

The distributions of the apparent central surface brightness of discs for edge-on view $\mu_{0,\mathrm{d}}$ corrected for Galactic extinction in the $JHK_s$ filters are shown in Fig. 5a. The values of this parameter span more than $3^m$ arcsec$^{-2}$ in each filter. The distributions shift from the filter $J$ to the filter $K_s$ with increasing of mean central surface brightness. It is well seen that LSB galaxies were not included in the sample. Thus, one has to keep in mind that in fact the number of such galaxies could be high at the faint end of the distribution of $\mu_{0,\mathrm{d}}$ in all three passbands.

Fig. 5b shows a large range in scalelengths $h$. Most of the sample galaxies have $h = 1 - 6$ kpc but the number of extended galaxies is small. The distributions of the disc scaleheight $z_0$ are shown in Fig. 5c. There is a fairly narrow distribution, that lies in the range $z_0 = 0.4 - 1.2$ kpc, and a tail of "thick" galaxies with $z_0 \gtrsim 1.2$ kpc. The shapes of distributions of $h$ and $z_0$ in each filter are quite similar and the median values of $h$ and $z_0$ have no systematic differences in the infrared bands under consideration (Table 4).

The statistical study of the ratio of the radial to the vertical scalelengths for galactic discs, $h/z_0$, gives constraints on kinematical and dynamical models of galaxies. The distribution of this ratio $h/z_0$ is shown in Fig. 5d. It is rather flat. The mean ratio $\langle h/z_0 \rangle$ is about 3.9 for the $H$ and $K_s$-bands (Table 6). Kregel et al. (2002) found the mean ratio of $\langle h/z_0 \rangle = 3.7 \pm 1.1$ (in the $I$-band) which is close to our result. For the sample of 153 galaxies composed by BM02 the mean ratio of $h/z_0$ is about 4.8. Although they studied galaxies in the $K_s$-band, their sample consists of late-type galaxies and the mean value of the ratio $h/z_0$ for these galaxies is larger than the mean ratio found in this paper. Apparently the mean $h/z_0$ ratio is higher in the blue filters than in the near-infrared bands (see for comparison e.g. van der Kruit & Searle 1982a and de Grijs & van der Kruit 1996).

#### *5.1.2 Bulges*

The distributions of the apparent effective surface brightness of bulges are shown in Fig. 5e. The distributions in each filter

[2] For NGC 5308 and NGC 1184 Bedregal et al. (2006) give the formal errors for the bulge effective radii that are very large and asymmetric. Unfortunately, they did not provide any explanation of these facts. For both galaxies, the bulge effective radii from our study and those by Bedregal et al. (2006) are quite different.

**Table 3.** Comparison between structural parameters obtained in this work and by Bedregal et al. (2006) in the $K_s$-band (parameters given in arcsec were rewritten in kpc according to distances adopted by Bedregal et al.).

| | This paper | | | Bedregal et al. (2002) | | |
|---|---|---|---|---|---|---|
| Name | $h$ (kpc) | $r_{e,b}$ (kpc) | $n$ | $h$ (kpc) | $r_{e,b}$ (kpc) | $n$ |
| NGC 5308 | 2.80± 0.89 | $1.53 \pm 0.10$ | $3.74 \pm 0.47$ | $2.68^{+0.12}_{-0.05}$ | $0.62^{+0.11}_{-2.51}$ | $2.99^{+0.04}_{-0.06}$ |
| NGC 1184 | $4.29 \pm 0.64$ | $1.84 \pm 0.06$ | $3.83 \pm 0.21$ | $3.80^{+0.06}_{-0.05}$ | $1.07^{+0.07}_{-2.43}$ | $3.58^{+0.07}_{-0.05}$ |
| NGC 4417 | $1.57 \pm 0.35$ | $0.86 \pm 0.03$ | $3.25 \pm 0.23$ | $1.82^{+0.04}_{-0.05}$ | $0.62^{+0.03}_{-0.02}$ | $2.79^{+0.07}_{-0.06}$ |
| NGC 1380A | $1.70 \pm 0.23$ | $0.53 \pm 0.02$ | $3.36 \pm 0.29$ | $1.80^{+0.04}_{-0.06}$ | $0.98^{+0.32}_{-0.25}$ | $3.71^{+0.07}_{-0.10}$ |
| NGC 1381 | $2.36 \pm 0.56$ | $0.88 \pm 0.03$ | $2.89 \pm 0.20$ | $1.88^{+0.07}_{-0.05}$ | $0.67^{+0.02}_{-0.01}$ | $3.07^{+0.14}_{-0.10}$ |

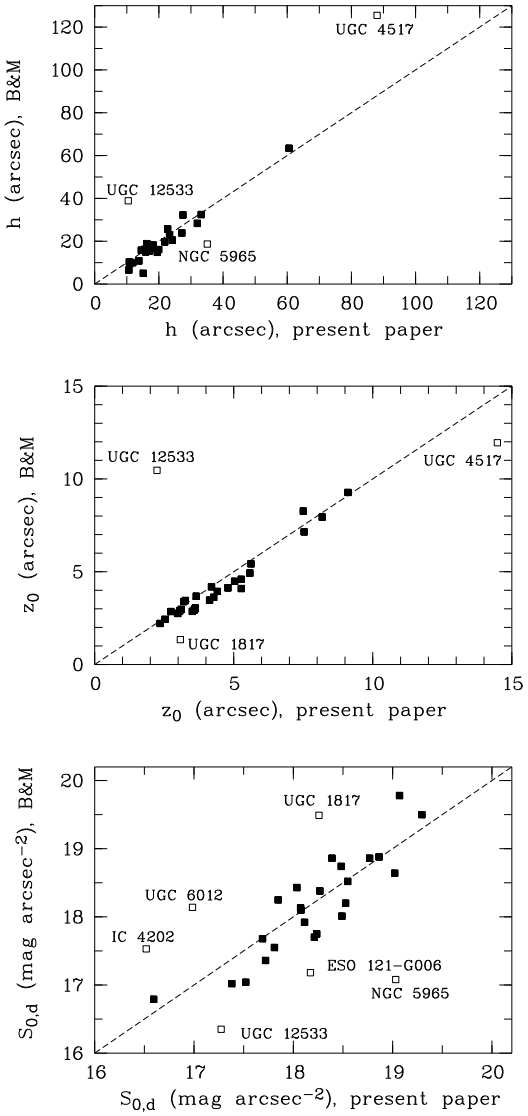


**Figure 3.** Comparison of the radial scalelengths (the upper frame), the vertical scaleheights (the middle frame) and the deprojected central surface brightnesses (the bottom frame) between data of BM02 and the data presented in this paper. Open squares are related to the galaxies with some peculiarities and features within their structure as noted in Sect.4.

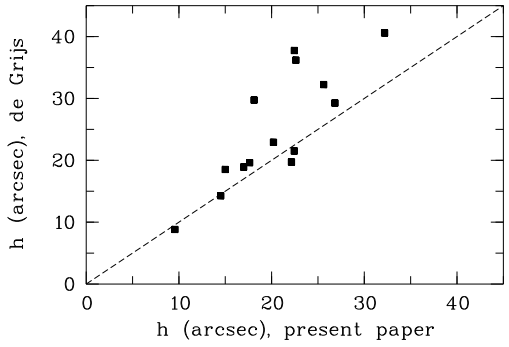


**Figure 4.** Comparison between radial scalelengths obtained by de Grijs (1998) and in this work.

have a narrow peak in contrast to the distributions of the central surface brightness of discs.

Fig. 5f demonstrates the fairly broad distributions of the effective radii of the bulges of galaxies. The distributions of the Sérsic indices of galaxies are shown in Fig. 5g. The distributions demonstrate a weak bimodality which may reflect the existence of two families of bulges: bulges with $n \gtrsim 2$ and bulges with $n \lesssim 2$. This bimodality is known for some galaxy samples (e.g. Fisher & Drory 2008) and probably is real for our sample. As was reported earlier (see e.g. Fisher & Drory 2007, 2008) such a bimodality correlates with morphological type of the bulge. Classical bulges have $n \gtrsim 2$ and so-called pseudobulges have $n \lesssim 2$, but this Sérsic index threshold can be considered only as an approximation to identify pseudobulges. Further we are showing the difference in the photometric planes for these two types of bulges.

In Fig. 5h we demonstrate the distributions of model bulge axis ratio $q_b = b/a$ for edge-on view. In the case of edge-on galaxies this parameter describes directly the bulge flatness and the intrinsic 3D structure of bulges if they are assumed to be oblate spheroids. The Table 6 gives the median value of this parameter $\sim 0.63$, independently of the band. This is in good agreement with Moriondo, Giovanardi & Hunt (1998) and Noordermeer & van der Hulst (2007). Moriondo et al. (1998) derived for their samples of 14 moderately inclined galaxies the median intrinsic axis ratio $q_b = 0.64$ while Noordermeer & van der Hulst (2007) gave the average value of $\langle q_b \rangle = 0.55 \pm 0.12$ for their sample of 21 early-type disc galaxies decomposed into contributions from a spheroidal bulge with a Sérsic profile and a flat disk. Thus, bulges are definitely nonspherical and flattened.

In recent years a great deal of new data has made

researchers revise the assumption that bulges are oblate spheroids. However, conclusions about intrinsic 3D shapes of bulges and their possible triaxiality are still somewhat controversial, despite the fact that such conclusions are thought to be crucial for testing different scenarios of galaxy formation. For galaxies at intermediate inclination angles misalignment between the bulge and the disk major axes indicates that bulges are probably triaxial (Bertola, Vietri & Zeiliger 1991). From the observed distribution function of apparent ellipticities and misalignment angles Bertola et al. (1991) determined the probability distribution function (PDF) of intrinsic axial ratios for 32 bulges of their sample. The peak of the PDF falls on the intrinsic equatorial axis ratio[3] $B/A = 0.95$ and bulge flattening $C/A = 0.65$. About one half of all bulges seems to be close to oblate, with the remainder being triaxial. Fathi and Peletier (2003) measured the bulge deprojected ellipticity in the equatorial plane that was obtained from the ellipse fitting the galaxy isophotes within a bulge region. One can estimate the median of $B/A$ from their distribution function as $0.7-0.8$ with smaller values attributed to more elongated bulges in late-type galaxies. Méndez-Abreu et al. (2008) also focused their attention on the intrinsic equatorial ellipticity of bulges. They reconstructed the PDF for the sample of 148 unbarred S0-Sb galaxies and obtained the value of $\langle B/A\rangle = 0.85$. This is consistent with findings by Bertola et al. (1991) and Fathi and Peletier (2003). However, in contrast to Fathi and Peletier (2003), Méndez-Abreu et al. (2008) did not find any significant differences in the shape of bulges between samples of early- and late-type galaxies.

Our sample of edge-on galaxies allows us to distinguish clearly the difference in the bulge equatorial ellipticities for early- and late-type galaxies. As a Sérsic index is correlated with the Hubble type (Andredakis, Peletier & Balcells 1995; Graham 2001; Möllenhof 2004) (as well as with the bulge morphology, dividing bulges into classical ones and pseudobulges; Fisher & Drory 2008) we divided our sample bulges between those with Sérsic index $n \gtrsim 2$ (early-type galaxies or classical bulges) and those with $n \lesssim 2$ (late-type galaxies or pseudobulges) using $K_s$ filter. As one can see in Fig. 6 for bulges with $n \gtrsim 2$ the distribution of $q_\mathrm{b}$ has a rather narrow peak at $q_\mathrm{b} \approx 0.65$. This may reflect the fact that bulges in early-type spirals are nearly oblate spheroids with moderate flattening. The distribution of $q_\mathrm{b}$ for bulges with $n \lesssim 2$ is very wide, spreading from flat bulges up to nearly spherical ones. Such a distribution may be attributed to definitely triaxial, near prolate bulges that are seen from different projections — along the major axis and perpendicular to it. But we can not exclude that triaxial shape of bulges in late-type galaxies may hide the presence of bars that thickened in the vertical direction during secular evolution. We are planning to investigate this question in more detail in a forthcoming paper.

Fig. 7 demonstrates the distributions of the ratio of bulge and disc luminosities $B/D \equiv L_\mathrm{b}/L_\mathrm{d}$. Our sample contains many early-type galaxies with $B/D \gtrsim 0.5$ and late-type galaxies with values of $B/D \lesssim 0.2$. For edge-on galaxies the ratio of $B/D$ is a key parameter in addition to $n$ for classifying spiral galaxies on the Hubble sequence because the spiral arms are not seen in this case (de Jong 1996; Graham 2001). Our sample also demonstrates a correlation between the ratios of $B/D$ and the Hubble morphological types $T$ taken from LEDA (Fig. 8a) that is in agreement with previous work (e.g., de Jong 1996; Graham 2001; Möllenhoff & Heid 2001; Hunt, Pierini & Giovanardi 2004; Möllenhoff 2004). However for edge-on galaxies morphological types are very subjective. Comparisons of the Hubble types given by different classifiers show an rms uncertainty in the type index of order 2 $T$-units (Lahav et al. 1995). Unfortunately there are errors in the bulge/disc decomposition. Therefore we use both approaches (type $T$ from LEDA and obtained $B/D$) for describing morphological types of edge-on galaxies. In some cases we will distinguish early- and late-type galaxies using the Sérsic index $n$ because there is a good correlation between $B/D$ and $n$ (Fig. 8b). This correlation is not new and was presented by many authors (e.g., Andredakis et al. 1995; Graham 2001; Möllenhoff & Heid 2001; Hunt et al. 2004).

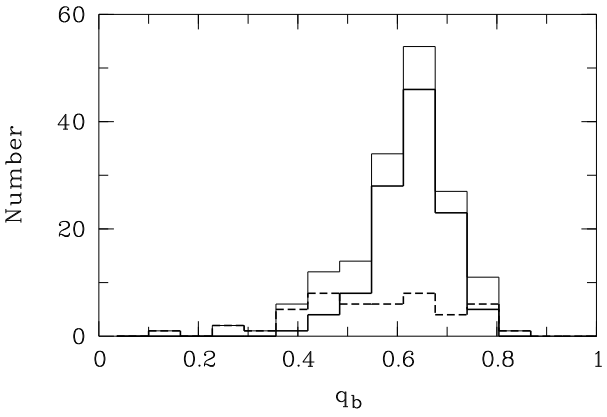


**Figure 6.** Distribution of the sample galaxies over the model bulge axis ratio $q_\mathrm{b}$ in the $K_s$-band. The thin line indicates the distribution for the whole sample, the solid line corresponds to the subsample of bulges with $n \gtrsim 2$ and the dashed line shows the distribution for the subsample of bulges with $n \lesssim 2$.

Details of the statistical properties of the sample discs and bulges are presented in the Table 4, the Table 5 and the Table 6. The values of $n$ in Table 5 systematically increase going from $J$ to $K_s$ – this may imply that $n$ is systematically underestimated due to extinction affecting the central peak of emission at the shorter near-IR wavelengths. Another possible explanation is a real change of the surface brightness shape with wavelength. But, as one can see in Table 5, the quoted changes are within statistical errors.

### 5.2 Scaling relations

The relationships between bulge and disc parameters might give an insight in the ages of the bulge and disc formation and help to reconstruct the chronology of these events. Andredakis & Sanders (1994) were the first to report the existence of a correlation between disc and bulge scalelengths

[3] We use capital letters $A$, $B$, $C$ to define the intrinsic semi-axes of a triaxial system and small letters $a$, $b$ for the apparent semi-axes of an image. In axisymmetric case and an edge-on view the ratio $b/a$ coincides with the ratio $C/A$.

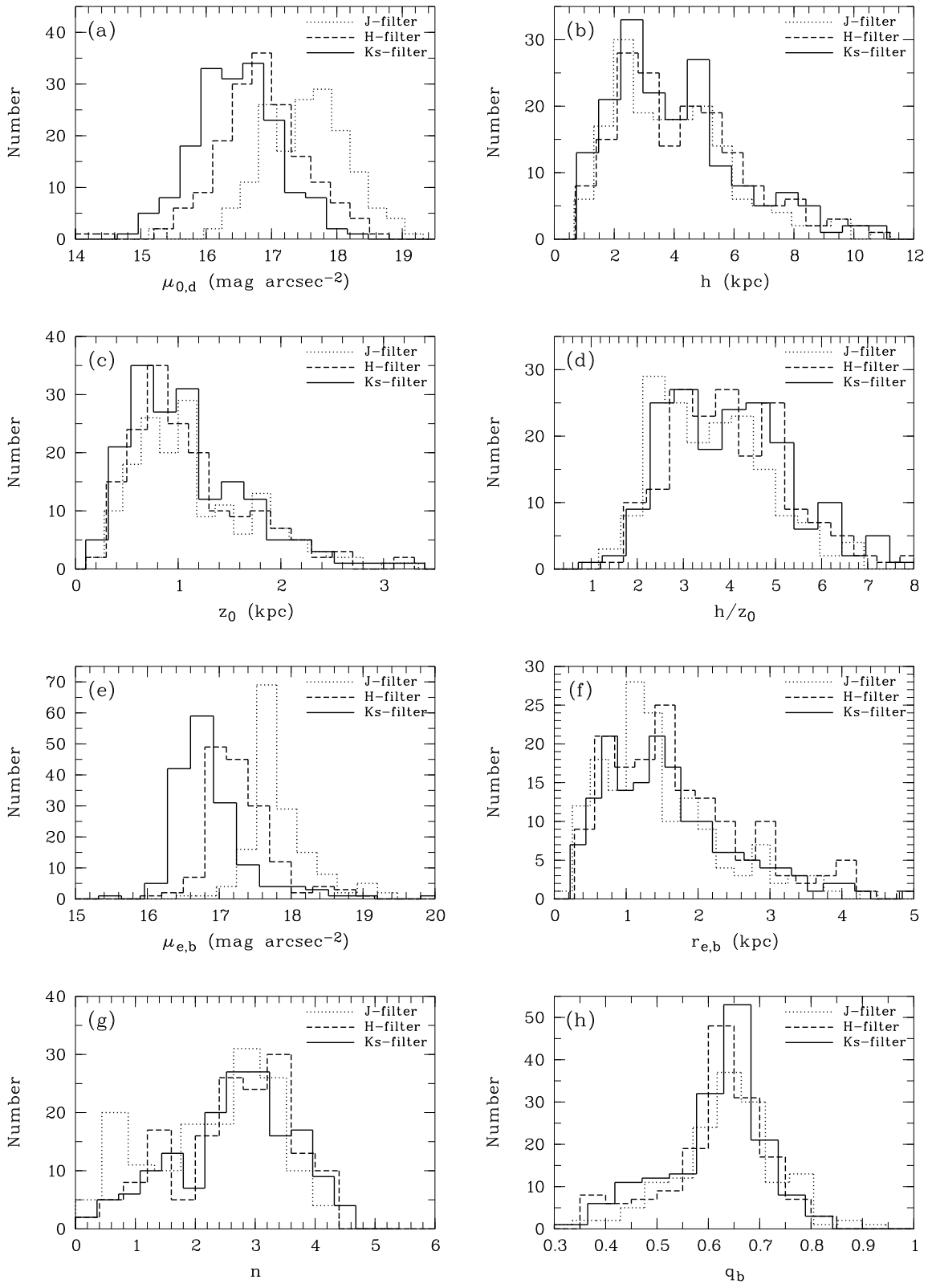


**Figure 5.** (a) Distributions of the sample galaxies over (a) the central surface brightness of the disc, (b) the disc scalelength, (c) the disc scaleheight, (d) the $h/z_0$ ratio, (e) the effective surface brightness of the bulge, (f) the bulge effective radius, (g) the Sérsic index of bulge, (h) the model bulge axis ratio $q_b = b/a$. In each plot the solid line corresponds to the $K_s$-band, the dashed line shows the distributions corresponds to the $H$-band and the dotted line corresponds to the $J$-band.

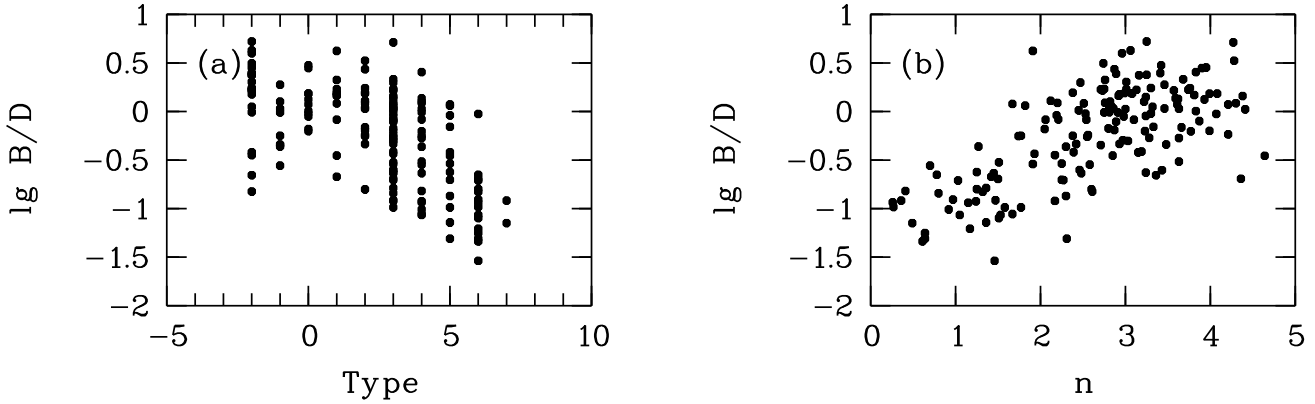


**Figure 8.** (a) The bulge to disc ratio as a function of the morphological type according to the RFGC (for late type galaxies RFGC provides more detailed dividing into types than LEDA), (b) the bulge to disc ratio versus the Sérsic index $n$ ($K_s$ passband).

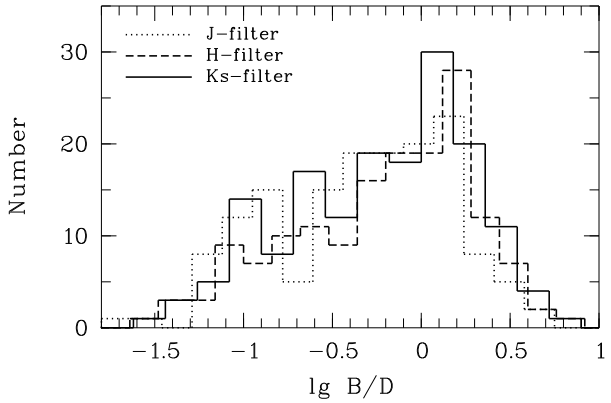


**Figure 7.** Distribution of the sample galaxies over the ratio bulge-to-disc luminosities $B/D = L_{\rm b}/L_{\rm d}$.

**Table 4.** The median values of $\mu_{0,\rm d}$, $h$, $z_0$ and $M_{\rm d}$ and their quartiles (75 and 25 per cent, respectively)

| Sp | $\mu_{0,\rm d}$ ($^m$/arcsec$^2$) | $h$ (kpc) | $z_0$ (kpc) | $M_{\rm d}$ ($^m$) |
|---|---|---|---|---|
| J | $17.57^{-0.55}_{+0.43}$ | $3.68^{-1.30}_{+1.44}$ | $1.04^{-0.34}_{+0.48}$ | $-22.53^{-0.77}_{+0.83}$ |
| H | $16.87^{-0.43}_{+0.35}$ | $3.87^{-1.36}_{+1.70}$ | $0.99^{-0.29}_{+0.45}$ | $-23.23^{-0.78}_{+0.82}$ |
| $K_s$ | $16.44^{-0.41}_{+0.43}$ | $3.66^{-1.27}_{+1.49}$ | $0.97^{-0.30}_{+0.45}$ | $-23.52^{-0.79}_{+0.75}$ |

for their sample of 34 late-type spirals. Just after that, such a correlation was confirmed and used for speculating about the scale-free Hubble sequence since the relative size of bulge and disc seemed not to depend on the morphological type (de Jong 1996; Courteau et al. 1996). De Jong (1996) found

**Table 5.** The median values of $\mu_{\rm e,b}$, $r_{\rm e,b}$, $n$ and $M_{\rm b}$ and their quartiles (75 and 25 per cent, respectively)

| Sp | $\mu_{\rm e,b}$ ($^m$/arcsec$^2$) | $r_{\rm e,b}$ (kpc) | $n$ | $M_{\rm b}$ ($^m$) |
|---|---|---|---|---|
| J | $17.68^{-0.13}_{+0.31}$ | $1.23^{-0.54}_{+0.55}$ | $2.35^{-1.36}_{+0.70}$ | $-21.97^{-0.97}_{+1.85}$ |
| H | $17.13^{-0.17}_{+0.36}$ | $1.48^{-0.63}_{+0.68}$ | $2.65^{-1.06}_{+0.68}$ | $-22.96^{-0.95}_{+1.93}$ |
| $K_s$ | $16.69^{-0.17}_{+0.34}$ | $1.35^{-0.59}_{+0.61}$ | $2.74^{-1.44}_{+0.53}$ | $-23.19^{-0.94}_{+2.16}$ |

**Table 6.** The median values of $h/z_0$, $q_{\rm b}$ and $B/D$ and their quartiles (75 and 25 per cent, respectively)

| Sp | $h/z_0$ | $q_{\rm b}$ | $B/D$ |
|---|---|---|---|
| J | $3.54^{-0.93}_{+0.86}$ | $0.63^{-0.07}_{+0.06}$ | $0.50^{-0.38}_{+0.62}$ |
| H | $3.94^{-0.85}_{+0.92}$ | $0.63^{-0.08}_{+0.05}$ | $0.69^{-0.49}_{+0.79}$ |
| $K_s$ | $3.92^{-0.92}_{+0.95}$ | $0.62^{-0.11}_{+0.04}$ | $0.64^{-0.44}_{+0.70}$ |

the equation for the least squares fitted line in the $K$ passband: $\lg(r_{\rm e,b}) = 0.95\lg(h) - 0.86$ with a standard deviation of 0.17 and correlation coefficient $r \sim 0.8$. This suggests a linear relation between $h$ and $r_{\rm e,b}$, i.e. the disc scalelength increases when the bulge effective radius increases.

Furthermore it became clear that the ratio $r_{\rm e,b}/h$ appeared to be strongly influenced by the bulge parametrization (Graham & Prieto 1999; Graham 2001). The independence of morphological type and a strong correlation were seen only when galaxies were best modeled with a fixed $n = 1$ bulges for all type galaxies (de Jong 1996; Courteau et al. 1996; Moriondo et. al. 1998; Hunt et al. 2004). According to whether bulges were fitted with the $n = 1$ Sérsic model or with the de Vaucoulers law, the correlation between scalelengths was clear or disappeared completely (Andredakis & Sanders 1994; de Jong 1996; Hunt et al. 2004).

Using Sérsic bulges with a free shape parameter $n$ as the best fitting models (Möllenhoff & Heidt 2001; Khosroshahi et al. 2000b; Graham 2001; MacArthur, Courteau & Holtzman 2003) or different but fixed $n$ for early- and late-type galaxies (Graham & Prieto 1999) confirms this correlation with a fairly large scatter and opens the discussion about the variation of the ratio $r_{\rm e,b}/h$ with Hubble types (Moriondo et al. 1998; Graham & Prieto 1999; Khosroshahi et al. 2000b; Graham 2001; Scodeggio et al. 2002; MacArthur et al. 2003; Möllenhoff 2004) and about the prematurity of the claims made by de Jong (1996) and Courteau et al. (1996) for a scale-free Hubble sequence.

We also found that there exist fairly strong correlations between structural parameters of discs and bulges. The correlation between $h$ and $r_{\rm e,b}$ is shown in Fig. 9a. In this figure and hereafter we mark the complete subsample galaxies with filled squares. The regression line is plotted only for points of the complete subsample. The equations of the linear re-

gression and the correlation coefficients are presented in the Table 7. These equations are consistent with a linear relation between $h$ and $r_{\rm e,b}$.

We found a mean $r_{\rm e,b}/h$ in the $J$-band of $0.39 \pm 0.18$, in the $H$-band of $0.42 \pm 0.20$ and in the $K_s$-band of $0.40 \pm 0.20$, which are in agreement within errors with the values obtained by Méndez-Abreu et al. (2008) for their sample of 148 unbarred S0–Sb galaxies $\langle r_{\rm e,b}/h \rangle = 0.36 \pm 0.17$ (in the $J$-band).

There is some controversial evidence for systematic changes with morphological type in the ratio $r_{\rm e,b}/h$ (Scodeggio et al. 2002; MacArthur et al. 2003; Hunt et al. 2004; Möllenhoff 2004). Despite being difficult to detect, the dependence with Hubble types might be real in the sense that the sample of predominantly late-type disk galaxies gives $\langle r_{\rm e,b}/h \rangle = 0.22 \pm 0.09$ (MacArthur et al. 2003; the $H$-band) and the sample of predominantly early-type galaxies leads to $\langle r_{\rm e,b}/h \rangle = 0.33 \pm 0.17$ (Khosroshahi et al. 2000b; the $K$-band).

For edge-on galaxies the reliable indicator of morphological type is $B/D$ or $n$. Fig. 9b demonstrates the dependence of the ratio $r_{\rm e,b}/h$ on the Sérsic shape parameter $n$. There is a clear trend for $r_{\rm e,b}/h$ to increase with $n$. The size ratio increases from $n \sim 0.5$ to $n \sim 5$ by a factor of $\sim 3-4$. Almost all bulges of the sample of MacArthur et al. (2003) have $n < 1.2$ and most of the bulges of the sample of Khosroshahi et al. (2000b) have $n > 2.2$. Thus, the difference in the mean value of $r_{\rm e,b}/h$ for these two samples reflects the same tendency that one can see in Fig. 9b. The same increase was declared by Hunt et al. (2004). They found for $n = 1$ bulges $\langle r_{\rm e,b}/h \rangle = 0.14 \pm 0.06$, for $n = 2$ bulges $\langle r_{\rm e,b}/h \rangle = 0.25 \pm 0.17$, for $n = 3$ bulges $\langle r_{\rm e,b}/h \rangle = 0.35 \pm 0.27$, and for $n = 4$ bulges $\langle r_{\rm e,b}/h \rangle = 0.54 \pm 0.54$.

Since $n$ is an indicator (in statistical sense) of morphological type, the changes of $r_{\rm e,b}/h$ with the shape of the bulge implies that Hubble sequence is not scale-free. The same conclusion has been recently made by Gadotti (2009) for his sample of nearly 1000 galaxies. Moreover, he was able to distinguish in his sample two subsamples of classical bulges and pseudobulges. Gadotti (2009) have used the Kormendy relation (Kormendy 1977) for identifying pseudobulges and bulges by their loci in the $\langle \mu_{\rm e,b} \rangle^4 - r_{\rm e,b}$ plane. The corresponding loci are quite different for these two types of bulges. Gadotti (2009) found that $r_{\rm e,b}/h$ for galaxies of both subsamples was clearly correlated with the bulge-to-total luminosity ratio, although the corresponding relations for pseudobulges and classical bulges were offset. As the bulge-to-total luminosity ratio is related to the morphological (Hubble) type of a galaxy, the existence of such relations rule out the hypothesis of a scale-free Hubble sequence. It means that the widely discussed secular evolution scenario of the bulge formation should be improved to include the variation of $r_{\rm e,b}/h$ with $n$ (or other indicators of the type) even in the case of pseudobulges.

The disc flattening can be measured directly only in edge-on galaxies. It is commonly expressed as the ratio of disc scaleheight $z_0$ to disc scalelength $h$. This ratio shows a weak trend with Hubble type (de Grijs 1998), but there is a fairly clear correlation between both scale parameters (e.g. Kregel et al. 2002). The result of Kregel et al. (2002) can be transformed into the mean value of $\langle h/z_0 \rangle = 3.7 \pm 1.1$ for the volume corrected distribution. Our data also demonstrates such a correlation for galaxies of all types (Fig. 10a). It is remarkable that the line of the linear regression is drawn through the point close to $(0, 0)$.

We used the data of photometric parameters $h$ and $z_0$ in BM02 ($K_s$ filter) of their reliable subsample and found the following equation of linear regression: $z_0 = (0.210 \pm 0.026)\, h - (0.017 \pm 0.258)$ with correlation coefficient $r = 0.727$, which is very close to our result (Table 7).

Thus, the galaxies with large disc scalelengths have on average larger disc scaleheights and larger effective radii of their bulges. However, one should keep in mind the fact that the spread in the $h - z_0$ plane is large. This scatter is reflected in a wide and remarkably flat distribution of the ratio $h/z_0$ presented in Fig. 5d. We return to this question in Section 5.5.

As is seen in Fig. 10b the disc scaleheight tends to increase with the bulge effective radius. The correlation between $z_0$ and $r_{\rm e,b}$ is new and was not described earlier. We found the following ratios of mean $r_{\rm e,b}/z_0$: $\langle r_{\rm e,b}/z_0 \rangle = 1.23 \pm 0.48$ for the $J$-band, $\langle r_{\rm e,b}/z_0 \rangle = 1.57 \pm 0.62$ for the $H$-band, $\langle r_{\rm e,b}/z_0 \rangle = 1.49 \pm 0.60$ for the $K_s$-band.

**Table 7.** The best fitting results for correlations between bulge and disc scale parameters

| | |
|---|---|
| $J$: | $\lg h = (1.011 \pm 0.143) \lg r_{\rm e,b} + (0.596 \pm 0.010)$, $r = 0.59$ |
| $H$: | $\lg h = (0.936 \pm 0.113) \lg r_{\rm e,b} + (0.533 \pm 0.030)$, $r = 0.66$ |
| $K_s$: | $\lg h = (0.933 \pm 0.104) \lg r_{\rm e,b} + (0.555 \pm 0.021)$, $r = 0.68$ |
| $J$: | $z_0 = (0.237 \pm 0.015)h + (0.010 \pm 0.140)$, $r = 0.87$ |
| $H$: | $z_0 = (0.208 \pm 0.014)h + (0.030 \pm 0.144)$, $r = 0.84$ |
| $K_s$: | $z_0 = (0.207 \pm 0.013)h + (0.027 \pm 0.129)$, $r = 0.85$ |
| $J$: | $z_0 = (0.891 \pm 0.120)r_{\rm e,b} + (0.058 \pm 0.356)$, $r = 0.62$ |
| $H$: | $z_0 = (0.680 \pm 0.100)r_{\rm e,b} + (0.045 \pm 0.366)$, $r = 0.59$ |
| $K_s$: | $z_0 = (0.715 \pm 0.094)r_{\rm e,b} + (0.041 \pm 0.325)$, $r = 0.61$ |

### 5.3 Well-known relationships

Here we investigate the general scaling relations for spiral galaxies such as the Tully-Fisher relation, the Fundamental Plane (FP) of discs and the Photometric Plane of bulges (PhP). In this subsection we study the Tully-Fisher relation and the Fundamental Plane of discs and in the next subsection we specially investigate the Photometric Plane of bulges.

#### *5.3.1 The Tully-Fisher relation*

The Tully-Fisher (TF) relation links the luminosity and the maximum rotation velocity $v_{\rm rot}$ of galaxies. The small scatter in the Tully-Fisher relation allows us to use it as a method for measurements of distances to spiral galaxies. To determine the slope and the zeropoint of the TF relation we used the total luminosities of the sample galaxies taken from 2MASS ($J_{\rm ext}$, $H_{\rm ext}$ or $K_{\rm ext}$). They were derived from the isophotal magnitudes by using the $K_s$-band 20 mag/arcsec$^2$ elliptical radius ($J_{20}$, $H_{20}$, $K_{20}$) and then were extrapolated to roughly four times the disc scalelength $h$ (for the detailed description see Jarrett et al. 2000 and Cutri et al. 2006).

[4] The mean effective surface brightness within the circle of effective radius $r_{\rm e,b}$.

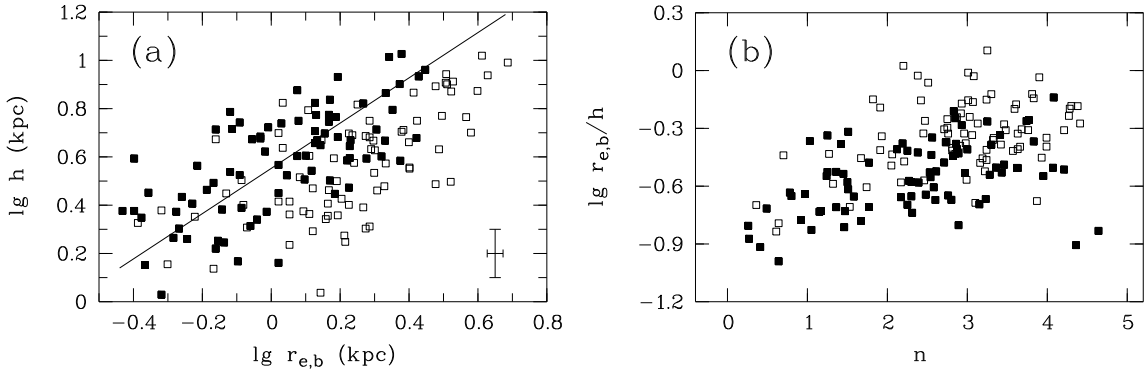


**Figure 9.** (a) The disc scalelength $h$ vs. the bulge effective radius $r_{\rm e,b}$, (b) $r_{\rm e,b}/h$ ratio vs. Sérsic index $n$ in the $K_s$-band. Open squares are related to the whole sample and the filled squares are related to the complete sample. The solid line corresponds to the regression line for the complete sample. The errorbars indicate the median error for all galaxies.

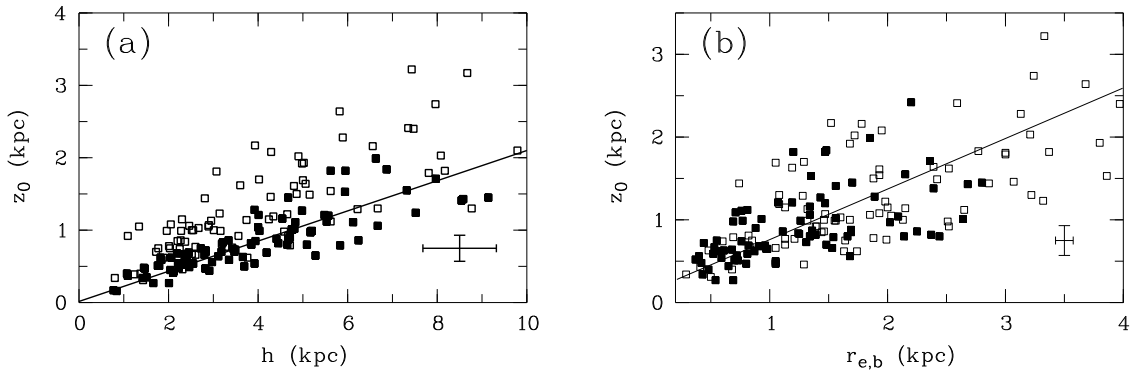


**Figure 10.** (a) The disc scaleheight $z_0$ vs. the disc scale length $h$, (b) the disc scale height $z_0$ vs. the bulge effective radius $r_{\rm e,b}$ ($K_s$). Symbols as in Fig. 9.

Unfortunately, measured rotation velocities are not known for all the sample galaxies. In the $J$-band the number of galaxies with known rotational velocities is 107, in the $H$-band there are 110 galaxies and in the $K_s$-band there are 116 objects with known velocities. The maximum rotational velocity corrected for inclination $v_{\rm rot}$ was taken from LEDA.

The absolute magnitude in different bands was calculated as

$$M_\lambda = m_\lambda - A_\lambda - 25 - 5\lg(D_{\rm L})\,, \qquad (10)$$

where $m_\lambda$ is the total apparent magnitude in each passband ($J_{\rm ext}$, $H_{\rm ext}$ or $K_{\rm ext}$), $D_{\rm L}$ is the luminosity distance and $A_\lambda$ is the Galactic extinction taken from Schlegel et al. (1998). The luminosity is expressed as

$$\lg L_\lambda = 0.4(M^\lambda_\odot - M_\lambda)\,, \qquad (11)$$

where $M^J_\odot = 3.64$ mag, $M^H_\odot = 3.32$ mag and $M^K_\odot = 3.28$ mag (Binney & Merrifield 1998). We fitted the TF relation coefficients by taking the bisector between the lines of linear regression obtained through the standard LSQ and inverse LSQ methods. The best fitting results are presented in the Table 9. The $K_s$-band TF relation is plotted in Fig. 11a.

There are many papers with the TF relation in the NIR bands for early- and late-type galaxies. Here we compare our results with those of some works based on 2MASS observations. The results by Karachentsev et al. (2002), Courteau et al. (2007), de Rijcke et al. (2007) and Masters, Springob & Huchra (2008) are presented in Table 8.

As was shown by Masters et al. (2008) the TF relation coefficients depend on galaxy morphology. The relationship is steeper for later type spirals than earlier type spirals. The TF zeropoint is dimmer for late-type galaxies. We did not divide our sample on morphological types to get the TF relation for various galactic types. Our sample contains an almost equal number of early- and late-type galaxies. That is why the coefficients found are somewhat different from those given in other papers.

### *5.3.2 The Fundamental Plane of discs*

Following Moriondo et al. (1999) we fit a relation for disc parameters as:

$$\lg h = a\lg v_{\rm rot} + b\,S_{0,\rm d} + c\,, \qquad (12)$$

involving the disc scalelength, the maximum rotational velocity, and the deprojected central surface brightness $S_0$, analogous to the FP of elliptical galaxies. To define coefficients of the linear approximation we used the standard least squares method. From the complete subsample we excluded 7 galaxies: NGC 7232 and NGC 5775 are interact-

**Table 8.** Comparison between some published 2MASS TF relations $\lg L = a \lg v_{\rm rot} + b$

| Reference | $J$-band | | $H$-band | | $K$-band | | Comments |
|---|---|---|---|---|---|---|---|
| | a | b | a | b | a | b | |
| This work | 3.43 | 2.67 | 3.44 | 2.83 | 3.55 | 2.66 | all types |
| Karachentsev et al. (2002) | 3.28 | | 3.48 | | 3.61 | | Based on $J_{\rm ext}$, $H_{\rm ext}$ and $K_{s,\rm ext}$, RFGC galaxies |
| Courteau et al. (2007) | 2.5 | 4.0 | 2.6 | 4.0 | 2.6 | 3.9 | 64% Sa galaxies |
| de Rijcke et al. (2007) | | | | | 3.46 | 2.44 | early-type galaxies |
| Masters et al. (2008) | 3.63 | 1.05 | 3.61 | 1.30 | 4.01 | 0.36 | Sc galaxies |
| Masters et al. (2008) | 3.12 | 2.32 | 3.12 | 2.53 | 3.45 | 1.76 | Sb galaxies |
| Masters et al. (2008) | 2.44 | 4.11 | 2.43 | 4.31 | 2.78 | 3.48 | Sa galaxies |

ing, NGC 7814 is a pure S0 galaxy with very faint disc, NGC 4222 and NGC 100 are low surface brightness galaxies, NGC 5023 and NGC 4183 have very large errors of disc parameters. The results of the fitting are given in Table 9. The scatter of points is rather large which may be caused by observational uncertainties and decomposition errors. The coefficients derived in this paper are comparable with those reported by Karachentsev (1989) for the $I$-band: $a = 1.4$, $b = 0.28$; and by Moriondo et al. (1999) for the $H$-band: $a = 1.31\pm0.19$, $b = 0.25\pm0.04$. Our coefficients as well as the coefficients derived by Karachentsev (1989) and Moriondo et al. (1999) are not consistent with what would be expected on the basis of the virial theorem and a universal mass-to-light ratio ($a = 2$ and $b = 0.4$).

We divided galaxies into galaxies with $n \gtrsim 2.2$ and galaxies with $n \lesssim 2.2$. In spite of the fact that the shape parameter $n$ is related to the bulge model, the fundamental planes of discs, which tie only disc parameters and the maximum rotational velocity of gas, are different for galaxies with different bulges. Perhaps it is due to observational errors and errors of decomposition for galaxies of different morphological types (for early-type galaxies rotational velocities and parameters of faint discs are less well defined than for late-type galaxies). Another reason may be the real difference of discs in galaxies with low and high density bulges. This effect requires a more careful examination.

### 5.4 Photometric Plane and Sérsic index

The Sérsic index $n$ represents the parameter quantifying the radial concentration of the stellar distribution of bulges. The detailed structure of bulges, their formation and evolutionary status is now widely discussed. Here we present a correlation between bulge absolute magnitude $M_{\rm b}$ and $n$. The plot is shown in Fig. 12a. The presented correlation is well-known (e.g. Andredakis et al. 1995; Graham 2001; Hunt et al. 2004; Möllenhoff & Heidt 2001; Möllenhoff 2004) and seen in all bands — from optical to near-infrared. It shows that exponential bulges are fainter than the de Vaucouleurs' bulges, although the scatter in the plot is large.

There are a lot of trends of galactic structural parameters with the Sérsic index of a bulge $n$, but the most prominent difference in parameters arises when one divides the sample under investigation into the subsample of classical bulges and pseudobulges. As was shown above, perhaps, the difference between classical bulges and pseudobulges is reflected in the intrinsic flattening and the 3D shape of bulges, in the ratio $r_{\rm e,b}/h$ and in building fundamental planes for discs.

The division of bulges into classical bulges and pseudobulges was described in many works (see Kormendy & Kennicutt 2004 for review). Classical bulges appear to be similar to elliptical galaxies and have similar properties. It is assumed that these systems were built via minor and major merging. The galaxies with pseudobulges are classified by the presence of some features within a bulge, e.g. nuclear bars, nuclear spirals and nuclear rings (Erwin & Spark 2002; Carollo et al. 1997; Fisher & Drory 2008). Pseudobulges are thought to be formed via disc instabilities and secular evolution and have disc-like apparent flattening. One of the main differences between classical bulges and pseudobulges is in the shape parameter $n$. Pseudobulges as usual have $n \lesssim 2$ and classical bulges have $n \geqslant 2$ with little-to-no overlap.

The images of galaxies under investigation have low resolution and inner features inside a bulge are smoothed. That is why we were searching for correlations between obtained structural parameters of the bulges with different Sérsic index $n$, not with morphological features. Here we describe the difference between bulges and pseudobulges while building the photometric plane for them.

Khosroshahi et al. (2000a,b) found a tight correlation of the Sérsic indices $n$ with the central surface brightness $\mu_{0,\rm b}$ and the effective radius of a bulge $r_{\rm e,b}$. They called this relationship the Photometric Plane.

Following Khosroshahi et al. (2000a,b) we performed the least-squared fit which expresses $\lg n$ as a linear combination of two other parameters: $\lg n = a \lg r_{\rm e} + b\,\mu_{0,\rm b} + c$. From the complete subsample we exclude galaxies with very small bulges and 2 bright flat galaxies of late types: NGC 4244 and NGC 4517.

For the complete sample the best fitting results are presented in Table 10. Khosroshahi et al. (2000a,b) found the Photometric Plane for 26 bulges of predominantly early-type galaxies in the $K$-band: $\lg n = (0.130 \pm 0.040) \lg r_{\rm e,b} - (0.073\pm0.011)\mu_{0,\rm b} + (1.21\pm0.11)$. Möllenhoff & Heidt (2001) obtained for their sample of 41 predominantly late-type spirals in the $JHK$ bands: $\lg n = 0.187 \lg r_{\rm e,b} - 0.081\mu_{0,\rm b} + 1.34 \pm 0.10$ with the correlation coefficient $r = 0.91$. Finally, Méndez-Abreu et al. (2008) gave $\lg n = 0.17(\pm0.02) \lg r_{\rm e,b} - 0.088(\pm0.004)\mu_{0,\rm b} + 1.48(\pm0.05)$ for their sample of 148 unbarred S0–Sb galaxies in the $J$-band. Within error bars, the differences between our coefficients for all our complete sample and those of Khosroshahi et al. (2000a,b), Möllenhoff & Heidt (2001) and Méndez-Abreu et al. (2008) are not significant, at least in the $K$-band.

The surprising result was the non-linear correlation of the PhP for galaxies with various values of $n$ (Fig. 12b). From our main sample we extracted the subsample of galaxies with $\lg n \gtrsim 0.2$ ($n \gtrsim 1.58$) and obtained the best-fit Photometric Plane (see Table 10). It occurred that the galax-

**Table 9.** The Tully-Fisher relations and disc fundamental planes for complete sample galaxies in the $J$, $H$, and $K_s$-bands. The fundamental planes are presented for all complete sample galaxies, for galaxies with $n \gtrsim 2.2$ and for galaxies with $n \lesssim 2.2$.

| |
|---|
| $J$: $\lg L = (3.43 \pm 0.29) \lg v_{\rm rot} + (2.67 \pm 1.39)$, $r = 0.82$ |
| $H$: $\lg L = (3.44 \pm 0.28) \lg v_{\rm rot} + (2.83 \pm 1.32)$, $r = 0.82$ |
| $K_s$: $\lg L = (3.55 \pm 0.30) \lg v_{\rm rot} + (2.66 \pm 1.41)$, $r = 0.81$ |
| For all galaxies of the complete sample with known velocities: |
| $J$: $\lg h = (1.017 \pm 0.101) \lg v_{\rm rot} + (0.173 \pm 0.021) S_{0,\rm d} - (5.04 \pm 0.11)$ |
| $H$: $\lg h = (1.044 \pm 0.092) \lg v_{\rm rot} + (0.190 \pm 0.020) S_{0,\rm d} - (5.28 \pm 0.11)$ |
| $K_s$: $\lg h = (1.077 \pm 0.104) \lg v_{\rm rot} + (0.202 \pm 0.023) S_{0,\rm d} - (5.53 \pm 0.12)$ |
| For galaxies of the complete sample with $n \gtrsim 2.2$: |
| $J$: $\lg h = (0.729 \pm 0.265) \lg v_{\rm rot} + (0.204 \pm 0.054) S_{0,\rm d} - (4.92 \pm 0.14)$ |
| $H$: $\lg h = (0.790 \pm 0.149) \lg v_{\rm rot} + (0.193 \pm 0.029) S_{0,\rm d} - (4.70 \pm 0.11)$ |
| $K_s$: $\lg h = (0.750 \pm 0.149) \lg v_{\rm rot} + (0.209 \pm 0.031) S_{0,\rm d} - (4.83 \pm 0.12)$ |
| For galaxies of the complete sample with $n \lesssim 2.2$: |
| $J$: $\lg h = (1.218 \pm 0.122) \lg v_{\rm rot} + (0.213 \pm 0.027) S_{0,\rm d} - (6.29 \pm 0.09)$ |
| $H$: $\lg h = (1.224 \pm 0.149) \lg v_{\rm rot} + (0.230 \pm 0.025) S_{0,\rm d} - (6.45 \pm 0.08)$ |
| $K_s$: $\lg h = (1.281 \pm 0.146) \lg v_{\rm rot} + (0.231 \pm 0.026) S_{0,\rm d} - (6.53 \pm 0.08)$ |

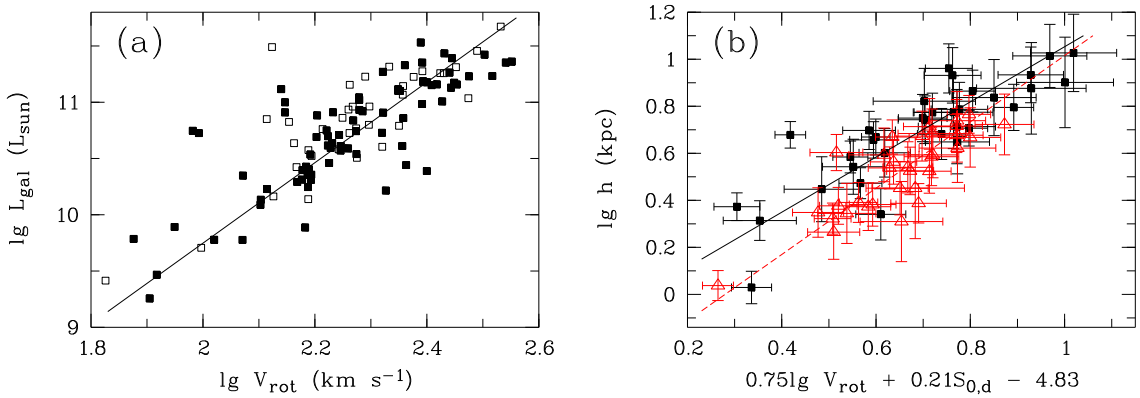


**Figure 11.** (a) The Tully-Fisher relation in the $K_s$-band. Symbols as in Fig. 9. (b) The disc fundamental plane for galaxies with $n \gtrsim 2.2$ in the $K_s$-band (filled squares). It is shown that galaxies with $n \lesssim 2.2$ compose a different fundamental plane. These galaxies are plotted with open triangles. Only galaxies of the complete sample are shown.

ies with $\lg n \gtrsim 0.2$ lying on the PhP, that is built for these galaxies, has a small scatter, but the galaxies with $\lg n \lesssim 0.1$ ($n \lesssim 1.26$) do not correspond to this plane and form their own plane (see Table 10). Inside the window $0.1 < \lg n \lesssim 0.2$ there are points which do not correspond to these two planes. The regression of the PhP is non-linear, but we approximate this dependence as a superposition of two linear regressions. The definite difference between the photometric planes of the bulges with different shape parameters $n$ is shown in Fig. 12b. The error bars are plotted as an indicator of the really different location of bulges and pseudobulges in the photometric planes. At a first glance the errors in the leftmost region of the plot are large, but bulges with very small $n$ are clearly recognized in surface brightness profiles of galaxies. What more, the relationship for bulges in the rightmost region of the plot begins to deviate from a linear trend for values of $n$ significantly above 1. The main difference between our sample and the samples of the above-mentioned authors is the range of the shape parameters $n$. Our sample contains a substantial amount of bulges with $\lg n \lesssim 0.1$. For other samples the low boundary for $n$ lies at $\lg n \gtrsim 0.2$, that is why the curvature of the Photometric Plane towards small values of $n$ for bulges was not noticed earlier.

This result is quite new and surprising. We realise that the points on the lower-left of the figure have bulges with $n < 1$, which are somewhat controversial and need further investigation, which will be done in a future paper. But a similar planar relation associated with the Photometric Plane was found for bright ellipticals, dwarf ellipticals and lenticular galaxies (Khosroshahi et al. 2000a; Khosroshahi et al. 2004; Ravikumar et al. 2006; Barway et al. 2009). If the range of the Sérsic parameter $n$ for ellipticals stretches to very small values of $n$, the curvature is clearly observed (Khosroshahi et al. 2004; Ravikumar et al. 2006).

The origin of the tight relation between $n$ and the linear combination of $\lg r_{\rm e}$ and $\mu_{0,\rm b}$ as well as the curvature of this relation are not completely clear. Aceves, Velásquez & Cruz (2006) argued that the curvature was related to an intrinsic property of a Sérsic profile. They wrote an expression for the total luminous matter associated with a Sérsic profile in log-space, involving $n$, $\lg r_{\rm e}$ and $\mu_{0,\rm b}$, and showed that for a set of galaxies with equal luminosities there were non-constant terms in this expression. These terms introduce a systematic change in a PhP-like expression.

It is not clear whether two distinct parts of a curve in Fig. 12b reflect the different origin of bulges lying in the cor-

responding regions. However, the collisionless merger remnants of disc galaxies obtained in $N$-body simulations and fitted by a Sérsic profile fairly well reproduce the slope of the PhP in the region of $\lg n \gtrsim 0.2$ (Aceves et al. 2006). We put on the data of Aceves et al. (2006) in our Fig. 12b and found the numerical data are consistent with our observational ones.

The curvature of the PhP towards small values of $n$ may reflect the quite different nature of such bulges, formed, for example, via secular evolution of discs. One of the signs of secular evolution is the presence of a bar or other structures (such as rings, double exponential discs). We have made the assumptions about the existence of a bar or other structures in our sample galaxies on the basis of the 1D surface brightness profiles along the major axis and on the residual images where additional components, that were not included in the decomposition, become apparent. The galaxies with or without bars are represented among the galaxies with $\lg n \gtrsim 0.2$ (classical bulges) as well as among the galaxies with $\lg n \lesssim 0.2$ (pseudobulges). So the shape of the PhP may describe the deeper nature of these objects. Márquez et al. (2001) have suggested a theoretical explanation of the PhP of ellipticals. They calculated the specific entropy of elliptical galaxies (Entropic Surface), took into account a scaling relation between the potential energy and mass (Energy-Mass Surface) and showed that the PhP arose as an intersection line of these two planes demonstrating a curvature consistent with the observational data in the limited range of values that has been considered for $n$. All these arguments may be valid for bulges of all types too.

### 5.5 The dark halo and disc flattening

In spite of a good correlation between the disc scalelength $h$ and the disc scaleheight $z_0$, the scatter of the ratio $h/z_0$ is fairly large. The ratio $h/z_0$ characterizes a relative thickness of a galaxy, or its flattening. Fig. 5d shows that $h/z_0$ varies from $\sim 8$ for thin galaxies to $1-2$ for plump discs. Disc flattening appears to correlate with the morphological type (e.g. de Grijs 1998) and the global HI content (Reshetnikov & Combes 1997). Late-type and gas-rich galaxies are, on average, thinner than early-type systems, but this correlation is rather weak. Although the discs seem to be larger and thicker with a higher maximum rotation (van der Kruit & de Grijs 1999; Kregel et al. 2002, 2005), the ratio $h/z_0$ is not correlated with the rotation velocity (Zasov et al. 2002; Kregel et al. 2002, 2005).

Zasov et al. (2002) and Kregel et al. (2005) found that the disc flattening shows a definite trend with the ratio of dynamical mass to disc luminosity provided the dynamical mass is defined as the total mass enclosed within the sphere of radius that is equal to four disc scalelengths: $\mathrm{M_{tot}} = 4hv^2_{\mathrm{rot}}/G$. The total mass includes the mass of the disc $\mathrm{M_d}$, the dark halo $\mathrm{M_h}$ and the bulge $\mathrm{M_b}$. So, the ratio of dynamical mass to disc luminosity determines the relative mass of a spherical component or the relative mass of the dark halo for bulgeless galaxies. The found correlation implies that relatively thinner discs in bulgeless galaxies tend to be embedded in more massive dark haloes.

Kregel et al. (2005) argued that the analytical collapse model of disc galaxy formation (White & Rees 1978; Fall & Efstathiou 1980; Blumenthal 1986; Mo, Mao & White 1998), the local Toomre's (1964) stability criterion for a disc and the suggestion about vertical dynamical equilibrium, provided the constant value of the ratio of the vertical to the radial velocity dispersion $\sigma_z/\sigma_R$, lead to the correlation between the disc flattening and the ratio of dynamical mass to disc luminosity.

Zasov et al. (2002) suggested that discs are marginally stable against the growth of perturbations in their planes and bending perturbations. This stability against bending perturbations means that the ratio $\sigma_z/\sigma_R$ must be larger than some analytical threshold: $\sigma_z/\sigma_R \gtrsim 0.3-0.4$ (Polyachenko & Shukhman 1977; Araki 1985). $N$-body simulations give a somewhat larger value for this threshold — $\sigma_z/\sigma_R \simeq 0.6-0.8$ (e.g. Sotnikova & Rodionov 2003, 2006). For a disc in vertical dynamical equilibrium Zasov, Makarov & Mikhailova (1991) and Zasov et al. (2002) deduced a simple expression for $h/z_0$. We rewrite it in the following form:

$$\frac{h}{z_0} \sim \frac{1}{[Q(\sigma_z/\sigma_R)]^2}\frac{\mathrm{M_{tot}}}{\mathrm{M_d}} \sim \frac{f_\lambda}{[Q(\sigma_z/\sigma_R)]^2}\frac{\mathrm{M_{tot}}}{L_d}\,, \qquad (13)$$

where $Q$ is Toomre's (1964) stability parameter, and $f_\lambda$ is the mass-to-luminosity ratio in a fixed band. The linear relation between the ratio $h/z_0$ and the ratio of dynamical mass (or dark halo mass) to disc luminosity arises for marginally stable discs with $Q$ and $\sigma_z/\sigma_R$ near their thresholds.

To verify a linear trend (13), obtained analytically, Zasov et al. (2002) studied two different samples of edge-on bulgeless galaxies with known structural parameters in the $R$ and $K_s$ bands. They used the HI line width $W_{50}$ as a measure of dynamical mass and concluded that discs become thinner with increasing mass fraction of their dark halos. For our sample, which contains a great many galaxies with massive bulges, we performed the same analysis.

Fig. 13a shows the distribution of the sample galaxies over the ratio of the dynamical mass to the stellar mass $\mathrm{M_*} = \mathrm{M_d} + \mathrm{M_b}$. We adopted mass-to-light ratios $f_J = 1.5$, $f_H = 1.0$, and $f_{K_s} = 0.8\ \mathrm{M_\odot}/L_\odot$ (McGaugh et al. 2000). These mass-to-light ratios are consistent with the maximum disk best fitting the rotation curves for bright galaxies (e.g. Bottema 1999). There is a hint of bimodality in Fig 13a. This may reflect the presence of two different families of galaxies with different bulges in our sample.

The distribution of the ratio $\mathrm{M_{tot}}/\mathrm{M_*}$ ranges over the values from $\sim 1$ to $\sim 8-10$. The distribution of the ratio $h/z_0$ is varying in the same range (Fig. 5d). As the relation (13) deals not only with the contribution of the dark halo to the total mass but with the relative mass of spherical components, including a bulge, we choose the ratio $\mathrm{M_{tot}}/\mathrm{M_d}$ to demonstrate a trend for the disc flattening with the relative mass of a spherical component (Fig. 13b and Table 11). We excluded 6 points from fitting of $\mathrm{M_{tot}}/\mathrm{M_d}$ vs. $h/z0$: NGC 7814, NGC 4222, NGC 5965, NGC 4183 and NGC 100, that have faint disc, and NGC 5981 with a prominent bar.

The scatter of points in Fig. 13b is rather large. It may be caused by uncertainties in velocities and mass-to-light ratio determinations, decomposition errors and disc relaxation processes, that can thicken a disc just above the threshold for marginal stability. But some of this scatter must be real. Sotnikova & Rodionov (2005) concluded that the presence of a compact bulge is enough to suppress the bending instability that leads to the disc thickness increasing. A series of $N$-body simulations with the same total mass of a spherical

**Table 10.** The Photometric Planes for bulges of the complete sample

| |
|---|
| For all galaxies of complete sample |
| $J$: $\lg n = (0.053 \pm 0.059)\lg r_{\rm e,b} - (0.101 \pm 0.004)\mu_{0,\rm b} + (1.63 \pm 0.06)$ |
| $H$: $\lg n = (0.106 \pm 0.047)\lg r_{\rm e,b} - (0.084 \pm 0.004)\mu_{0,\rm b} + (1.37 \pm 0.05)$ |
| $K_s$: $\lg n = (0.160 \pm 0.058)\lg r_{\rm e,b} - (0.084 \pm 0.005)\mu_{0,\rm b} + (1.34 \pm 0.07)$ |
| $\lg n \geqslant 0.2$ |
| $J$: $\lg n = (0.030 \pm 0.018)\lg r_{\rm e,b} - (0.067 \pm 0.002)\mu_{0,\rm b} + (1.23 \pm 0.03)$ |
| $H$: $\lg n = (0.018 \pm 0.014)\lg r_{\rm e,b} - (0.062 \pm 0.002)\mu_{0,\rm b} + (1.14 \pm 0.02)$ |
| $K_s$: $\lg n = (0.022 \pm 0.013)\lg r_{\rm e,b} - (0.061 \pm 0.002)\mu_{0,\rm b} + (1.11 \pm 0.02)$ |
| $\lg n \lesssim 0.1$ |
| $J$: $\lg n = (0.137 \pm 0.134)\lg r_{\rm e,b} - (0.142 \pm 0.039)\mu_{0,\rm b} + (2.31 \pm 0.67)$ |
| $H$: $\lg n = (0.201 \pm 0.162)\lg r_{\rm e,b} - (0.172 \pm 0.051)\mu_{0,\rm b} + (2.76 \pm 0.83)$ |
| $K_s$: $\lg n = (0.467 \pm 0.214)\lg r_{\rm e,b} - (0.204 \pm 0.075)\mu_{0,\rm b} + (3.21 \pm 1.19)$ |

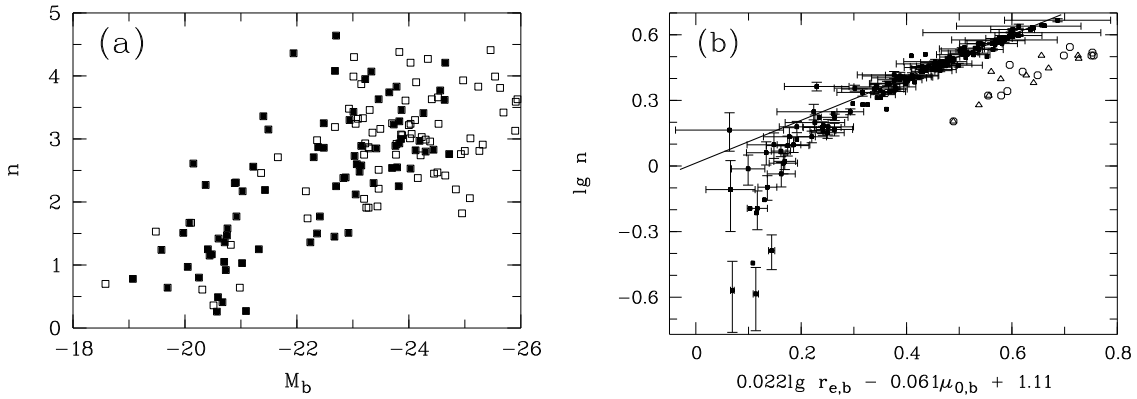


**Figure 12.** (a) Bulge Sérsic index $n$ vs. bulge absolute magnitude in the $K_s$-band. Symbols as in Fig. 9. (b) The Photometric Plane built for bulges with $\lg n \geqslant 0.2$ of the complete subsample in the $K_s$-band. The points corresponding to bulges with $\lg n \lesssim 0.1$ do not lie in this plane. The model merger remnants of disc galaxies are shown with open circles and triangles (Aceves et al. 2006). The model data are shifted by a constant along the horizontal axis.

**Table 11.** Correlations between $z_0/h$ and $\rm M_{tot}/M_d$

| |
|---|
| $J$: $h/z_0 = (0.634 \pm 0.100)\rm M_{tot}/M_d + (1.63 \pm 1.16)$, $r = 0.58$ |
| $H$: $h/z_0 = (0.696 \pm 0.120)\rm M_{tot}/M_d + (1.76 \pm 1.51)$, $r = 0.51$ |
| $K_s$: $h/z_0 = (0.756 \pm 0.135)\rm M_{tot}/M_d + (1.79 \pm 1.92)$, $r = 0.46$ |

component (dark halo + bulge) were performed. The final disc thickness was found to be much smaller in the simulations, where a dense bulge is present, than in the simulations with bulgeless systems. The results of $N$-body simulations of discs starting from an unstable state were summarized by Sotnikova & Rodionov (2006). They plotted the ratio $z_0/h$ versus $(\rm M_h + M_b)/M_d$ and showed that there is a clear scatter in this relation, in spite of the same model mass for a spherical component ($\rm M_h + M_b$). We are planning to compare in details our observational data with the results of simulations in a forthcoming paper.

## 6 SUMMARY AND CONCLUSIONS

We constructed the largest sample of edge-on spiral galaxies with performed 2D bulge/disc decomposition of 2MASS galaxies images in $J$-, $H$- and $K_s$-passband using the BUDDA v2.1 package. We extracted global bulge and disc parameters for all objects. This first paper describes our edge-on galaxy sample. The main point of this work is in the first carefully fitting of edge-on spiral galaxies of early and late morphological types in 3 near-infrared bands.

Edge-on galaxies are of great interest because they provide a unique possibility to obtain information about the vertical structure of a disk and a bulge. The disc scaleheight $z_0$ together with the disc scalelength $h$ determine the relative thickness of a stellar disc for each galaxy. This ratio as well as the bulge flattening $q_{\rm b}$ may put constraints on the disc and bulge formation processes and their secular evolution.

The results of the sample parameter analysis, that are specific for edge-on galaxies, can be summarized as follows:

(i) Our data demonstrate a clear correlation between the disc scaleheight $z_0$ and the disc scalelength $h$ for all type galaxies. The distributions of the sample galaxies over the ratio of $h/z_0$ have a median value of 3.5 for $J$-band and 3.9 for $H$ and $K_s$-bands. But there is a substantial scatter of this ratio (the distribution is fairly flat). The ratio $h/z_0$ stretches over a large range — from very thin galaxies to plump ones. There is a correlation between the relative thickness of stellar discs $h/z_0$ and the relative mass of a

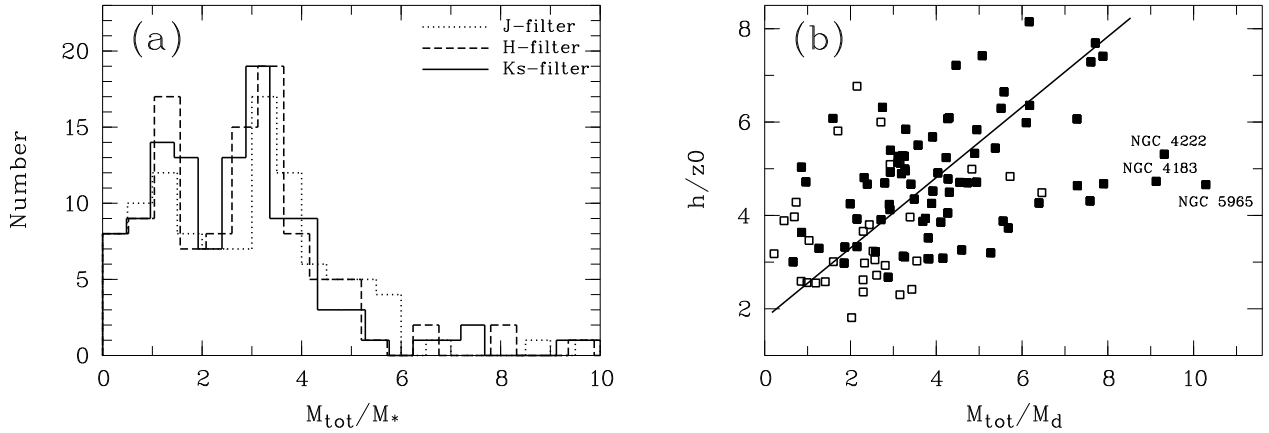


**Figure 13.** (a) Distribution of the sample galaxies over the ratio of dynamical mass to stellar mass of the galaxy. (b) The ratio of $h/z_0$ as a function of the ratio of dynamical mass to disc mass. Symbols as in Fig 9.

spherical component, including a dark halo. This correlation was known previously for bulgeless galaxies (Zasov et al. 2002) or samples with predominantly bulgeless galaxies (Kregel et al. 2005) and was argued to arise from marginally stable discs. Our sample is much larger than the samples of Zasov et al. (2002) and Kregel et al. (2005) and more reliable for statistical analysis. Here, we confirm the correlation under discussion. What is more, we do this not for bulgeless galaxies but for galaxies with massive bulges. We conclude that the *total* mass contained in spherical components may be one of the factors that determines the final steady state disc thickness.

(ii) The bulge flattening in the vertical direction $q_{\rm b}$ divides the sample into two different families — triaxial, nearly prolate bulges and close to oblate bulges with moderate flattening. The Sérsic index threshold $n \simeq 2$ can be used to identify these two bulge types.

(iii) We found a correlation between $z_0$ and $r_{\rm e,b}$. It is new and has not been described previously. It means that the disc flattening is linked with the bulge structure.

Many of our results are in good agreement with the results of other authors, but we found several new relations.

(i) In accordance with previous studies we found that the scale parameters of bulges and discs are tightly correlated. The disc scalelength linearly increases when the bulge effective radius increases. However, there is a clear trend for the ratio $r_{\rm e,b}/h$ to increase with $n$. As $n$ is an indicator of the Hubble type, such a trend unambiguously rules out the widely discussed hypothesis of a scale-free Hubble sequence.

(ii) There is a hint that the fundamental planes of discs, which link only disc parameters and the maximum rotational velocity of gas, are different for galaxies with different bulges. This may indicate a real difference of discs in galaxies with low and high density bulges.

(iii) The most surprising result arises from the investigation of the Photometric Plane of sample bulges. The bulges with $n \gtrsim 2$ populate a narrow strip in their Photometric Plane. However, there is a difference in behavior of this plane for bulges with $n \gtrsim 2$ and $n \lesssim 2$. The plane is not flat and has a prominent curvature towards small values of $n$. For bulges this fact was not noticed earlier. This result may be due to the physical distinction between classical bulges and pseudobulges. As the Photometric Plane is proposed to be used as a distance indicator, the correct shape of the plane is of no little interest.

Some of results were described only briefly, but it is clear that our sample is very useful for further detailed studying and modelling of edge-on spiral galaxies. In the forthcoming papers we are planning to discuss properties of edge-on galaxies in more detail in the context of their bulge and disc formation and joint evolution.

## ACKNOWLEDGMENTS

We thank R.E. de Douza, D.A. Gadotti and S. dos Anjos for getting the last version of code BUDDA. We especially thank D.A. Gadotti for the helpful comments to this program. We are indebted to the referee, Phil James, for his constructive comments and insightful suggestions which helped to improve the quality and the presentation of the paper.

This work was supported by the Russian Foundation for Basic Research (grant 09-02-00968) and by a grant from President of the RF for support of Leading Scientific Schools (grant NSh-1318.2008.02).

This research has made use of the NASA/IPAC Extragalactic Database (NED) which is operated by the Jet Propulsion Laboratory, California Institute of Technology, under contract with the National Aeronautics and Space Administration. We made use of the LEDA database (http://leda.univ-lyon1.fr).

## REFERENCES

Aceves H., Velázquez H., Cruz F., 2006, MNRAS, 373, 632
Andredakis Y.C., Sanders R.H., 1994, MNRAS, 267, 283
Andredakis Y.C., Peletier R.F., Balcells M.J., 1995, MNRAS, 275, 874
Araki S., A theoretical Study of the Stability of Disk Galaxies and Planetary Rings, PhD Thesis, Massachus. Inst. Tech., 1985

Baggett W.E., Baggett S.M., Anderson K.S.J., 1998, AJ, 116, 1626
Barteldrees A., Dettmar R.-J., 1994, A&AS, 103, 475
Bedregal A.G., Aragon-Salamanca A., Merrifield M.R., 2006, MNRAS, 373, 1125
Bertola F., Vietri M., Zeilinger W.W., 1991, ApJ, 374, L13
Binney J., Merrifield M., 1998, Galactic Astronomy, Princeton Univ. Press, Princeton
Bizyaev D., Mitronova S., 2002, A&A, 389, 795 (BM02)
Blumenthal G.R., Faber S.M., Flores R., Primack J.R., 1986, ApJ, 301, 27
Boroson T., 1981, ApJS, 46, 177
Bottema R., 1999, A&A, 348, 77
Byun Y.I., Freeman K.C., 1995, ApJ, 448, 563
Castro-Rodriguez N. Garzón F., 2003, A&A, 411, 55
Courteau S., de Jong R.S., Broeils A.H., 1996, ApJ, 457, 73
Courteau S., Dutton A.A., van den Bosch F.C., Mac Arthur L.A., Dekel A., McIntosh D.H., Dale D.A., 2007, ApJ, 671, 203
Cutri R.M., Skrutskie M.F., Van Dyk S., et al., 2006, Explanatory Supplement to the 2MASS All Sky Data Release and Extended Mission Products, http://www.ipac.caltech,edu/2mass/releases/allsky/doc/
Dalcanton J.J., Bernstein R.A., 2000, AJ, 120, 203
Dalcanton J.J., Bernstein R.A., 2002, AJ, 124, 1328
de Grijs R., 1998, MNRAS, 299, 595
de Grijs R., van der Kruit P.C., 1996, A&AS, 117, 19
de Jong R.S., 1996, A&A, 313, 45
de Rijcke S., Zeilinger W.W., Hau G.K.T., Prugniel P., Dejonghe H., 2007, ApJ, 659, 1172
de Vaucouleurs, 1948, Annales d'Astrophysique, 11, 247
de Vaucouleurs, 1953, MNRAS, 113, 134
de Vaucouleurs, 1959, Hdb. d. Physik, 53, 311
D'Onofrio M., Fasano G., Varela J., Bettoni D., Moles M., Kjærgaard P., Pignatelli E., Poggianti B., Dressler A., Cava A., Fritz J., Couch W.J., Omizzolo A., 2008, ApJ, 685, 875
de Souza R.E., Gadotti D.A., dos Anjos S., 2004, ApJS, 153, 411 (SGA04)
Erwin P., Sparke L.S., 2002, AJ, 124, 65
Faber S.M., Jackson R.E., 1976, ApJ, 204, 668
Fall S.M., Efstatiou G., 1980, MNRAS, 193, 189
Fathi K., Peletier R.F., 2003, A&A, 407, 61
Fisher D.B., Drory N., 2007, ApJ, 664, 640
Fisher D.B., Drory N., 2008, AJ, 136, 773
Fraser C.W., 1972, Observatory, 92, 51
Freeman K.C., 1970, ApJ, 160, 811
Gadotti D.A., 2009, MNRAS, 393, 1531
Graham A.W., 2001, AJ, 121, 820
Graham A.W., Prieto M., 1999, ApJ, 524, L23
Hunt L.K., Pierini D., Giovanardi C., 2004, A&A, 414, 905
Jarrett T.H., 2000, PASP, 112, 1008
Jarrett T.H., Chester T., Cutri R., Schneider S., Skrutskie M., Huchra J.P., 2000, AJ, 119, 2498
Karachentsev I.D., 1989, AJ, 97, 1566
Karachentsev I.D., Karachentseva V.E., Kudrya Yu.N., Sharina M.E., Parnovskij S.L., 1999, Bull. Spec. Astrophys. Obs., 47, 185
Karachentsev I.D., Mitronova S.N., Karachentseva V.E., Kudrya Yu.N., Jarrett T.H., 2002, A&A, 396, 431
Kent S.M., 1985, ApJS, 59, 115
Khosroshahi H.G., Wadadekar Y., Kembhavi A., Mobasher B., 2000a, ApJ, 531, L103
Khosroshahi H.G., Wadadekar Y., Kembhavi A., 2000b, ApJ, 533, 162
Khosroshahi H.G., Raychaudhury S., Ponman T.J., Miles T.A., Forbes D.A., 2004, MNRAS, 349, 527
Kormendy J., 1977, ApJ, 218, 333
Kormendy J., Kennicutt Jr. R.C., 2004, ARAA, 42, 603
Kregel M., Structure and Kinematics of Edge-on Galaxy Disks, PhD Thesis, Univ. Groningen, 2003
Kregel M., van der Kruit P.C., de Grijs R., 2002, MNRAS, 334, 646
Kregel M., van der Kruit P.C., Freeman K.C., 2005, MNRAS, 358, 503
Lahav O., Naim A., Buta R.J., Corwin H.G., de Vaucouleurs G., Dressler A., Huchra J.P., van den Bergh S., Raychaudhury S., Sodre L., Jr., Storrie-Lombardi M.C., 1995, Science, 267, 859
Laurikainen E., Salo H., Buta R., 2005, MNRAS, 362, 1319
MacArthur L.A., Courteau S., Holtzman J.A., 2003, ApJ, 582, 689
Márquez I., Lima Neto G.B., Capelato H., Durret F., Lanzoni B., Gerbal D., 2001, A&A, 379, 767
Masters K.L., Springob C.M., Huchra J.P., 2008, AJ, 135, 1738
McGaugh S.S., Schombert J.M., Bothun G.D., de Blok W.J.G., 2000, ApJ, 533, L99
Mitronova S.N., Karachentsev I.D., Karachentseva V.E., Jarrett T.H., Kudrya Yu.N., 2003, Bull. Spec Astrophys. Obs., 57, 5
Méndez-Abreu J., Aguerri J.A.L., Corsini E.M., Simonneau E., 2008, A&A, 478, 353
Mo H.J., Mao S., White S.D.M., 1998, MNRAS, 295, 319.
Möllenhoff C., 2004, A&A, 415, 63
Möllenhoff C., Heidt J., 2001, A&A, 368, 16
Moffat A.F.J., 1969, A&A, 3, 455
Moriondo G., Giovanardi C., Hunt L.K., 1998, A&AS, 130, 81
Moriondo G., Giovanelli R., Haynes M.P., 1999, A&A, 346, 415
Nakamura O., Fukugita M., Yasuda N., Loveday J., Brinkmann J., Schneider D., Shimasaku K., SubbaRao M., 2003, AJ, 125, 1682
Noordermeer E., van der Hulst J.M., 2007, MNRAS, 376, 1480
Reshetnikov V., Combes F., 1997, A&A, 324, 80
Sérsic J.L., 1968, Atlas de Galaxias Australes, Observatorio Astronomico, Cordoba
Schlegel D.J., Finkbeiner D.P., Davis M., 1998, ApJ, 500, 525
Schmidt M., 1968, ApJ, 151, 393
Scodeggio M., Gavazzi G., Franzetti P., Boselli A., Zibetti S., Pierini D., 2002, A&A, 384, 812
Seth A.C., Dalcanton J.J., de Jong R.S., 2005, AJ, 130, 1574
Skrutskie M.F., Cutri R.M., Stiening R., et al., 2006, AJ, 131, 1163
Sotnikova N.Ya., Rodionov S.A., 2003, Astr. Lett., 29, 321
Sotnikova N.Ya., Rodionov S.A., 2005, Astr. Lett., 31, 15
Sotnikova N.Ya., Rodionov S.A., 2006, Astr. Lett., 22, 649
Strateva I., Ivezić Ž., Knapp G.R., et al., 2001, AJ, 122, 1861

Thuan T.X., Seitzer P.O., 1979, ApJ, 231, 680
Toomre A., 1964, ApJ, 139, 1217
van der Kruit P.C., Searle L., 1981, A&A, 95, 105
van der Kruit P.C., de Grijs R., 1999, A&A, 352, 129
White S.D.M., Rees M.J, 1978, MNRAS, 183, 341
Yoachim P., Dalcanton J.J., 2005, ApJ, 624, 701
Zasov A.V., Makarov D.I., Mikhailova E.A., 1991, Astron. Lett., 17, 374
Zasov A.V., Bizyaev D.V., Makarov D.I., Tyurina N.V., 2002, Astron. Lett., 28, 527

**Table 1.** The Sample.

| # | Galaxy | 2MFGC | Type | $D$ (Mpc) |
|---|---|---|---|---|
| | (1) | (2) | (3) | (4) |
| 1 | UGC 529 | 633 | S0-a | 70.4 |
| 2 | NGC 504 | 1059 | S0 | 53.2 |
| 3 | NGC 527 | 1070 | S0-a | 74.7 |
| 4 | NGC 565 | 1133 | Sa | 57.0 |
| 5 | UGC 1120 | 1193 | Sab | 58.8 |
| 6 | ESO 353-G020 | 1202 | S0-a | 61.7 |
| 7 | UGC 1166 | 1243 | S0-a | 60.8 |
| 8 | ESO 013-G024 | 1422 | Sab | — |
| 9 | UGC 1531 | 1557 | Sb | 105.0 |
| 10 | IC 207 | 1660 | S0-a | 62.1 |
| 11 | NGC 861 | 1758 | Sb | 106.0 |
| 12 | UGC 1938 | 1930 | Sbc | 82.0 |
| 13 | NGC 955 | 1965 | Sab | 17.0 |
| 14 | NGC 960 | 1984 | Sb | 63.1 |
| 15 | MCG-02-07-038 | 2044 | S0 | 62.2 |
| 16 | NGC 1029 | 2102 | S0-a | 46.0 |
| 17 | UGC 2304 | 2260 | Sbc | 93.7 |
| 18 | MCG-02-09-013 | 2605 | S0-a | 61.2 |
| 19 | ESO 005-G004 | 4913 | Sb | 26.1 |
| 20 | NGC 1381 | 2983 | S0 | 22.2 |
| 21 | NGC 1394 | 3025 | S0 | 55.5 |
| 22 | NGC 1401 | 3030 | S0 | 18.8 |
| 23 | NGC 4256 | 9696 | Sb | 35.7 |
| 24 | MCG-02-08-012 | 2274 | Sc | 68.8 |
| 25 | NGC 1529 | 3366 | S0 | 68.7 |
| 26 | UGC 7388 | — | SBb | 89.8 |
| 27 | ESO 251-G028 | 3869 | Sb | 158.0 |
| 28 | NGC 4866 | 10288 | S0-a | 31.2 |
| 29 | ESO 555-G023 | 4860 | S0-a | — |
| 30 | ESO 555-G032 | 4905 | Sb | — |
| 31 | ESO 087-G004 | 5097 | Sbc | 118.0 |
| 32 | UGC 4012 | 6163 | Sb | 130.0 |
| 33 | UGC 4190 | 6390 | S0 | 69.9 |
| 34 | UGC 4507 | 6803 | Sb | 141.0 |
| 35 | UGC 4526 | 6822 | Sab | 62.4 |
| 36 | ESO 433-G012 | 7223 | Sbc | 115.0 |
| 37 | ESO 373-G013 | 7473 | S0-a | 40.7 |
| 38 | NGC 2946 | 7484 | SBb | 122.0 |
| 39 | UGC 5345 | 7714 | Sb | 53.5 |
| 40 | IC 615 | 8108 | Sb | 133.0 |
| 41 | ESO 501-G056 | 8260 | S0 | 53.0 |
| 42 | NGC 3431 | 8449 | SABb | 75.3 |
| 43 | MCG-01-28-005 | 8496 | Sab | 91.0 |
| 44 | CGCG 267-039 | 8658 | Sb | 88.2 |
| 45 | NGC 3539 | 8691 | S0-a | 132.0 |
| 46 | NGC 1184 | 2685 | S0-a | 30.8 |
| 47 | NGC 4149 | 9578 | Sb | 43.4 |
| 48 | MCG-02-32-006 | 9725 | SBc | 60.0 |
| 49 | NGC 4686 | 10067 | Sa | 69.5 |
| 50 | MCG-02-33-076 | 10273 | Sab | 47.0 |
| 51 | UGC 8119 | 10315 | Sbc | 117.0 |
| 52 | IC 844 | 10368 | S0 | 43.6 |
| 53 | MCG-01-33-076 | 10374 | Sc | 58.4 |
| 54 | IC 5096 | 16137 | Sbc | 41.2 |
| 55 | IC 881 | 10662 | Sa | 96.9 |
| 56 | NGC 5119 | 10737 | S0-a | 43.6 |
| 57 | UGC 8462 | 10813 | Sab | 132.0 |
| 58 | UGC 8704 | 11102 | Sa | 140.0 |
| 59 | NGC 5290 | 11096 | Sbc | 37.4 |
| 60 | NGC 5553 | 11621 | Sa | 63.8 |

**Table 1.** continued.

| # | Galaxy | 2MFGC | Type | $D$ (Mpc) |
|---|---|---|---|---|
| | (1) | (2) | (3) | (4) |
| 61 | ESO 384-G014 | 11249 | S0 | 57.2 |
| 62 | IC 1110 | 12300 | Sa | 46.0 |
| 63 | ESO 387-G029 | 12429 | Sab | 60.6 |
| 64 | UGC 11060 | 14135 | Sa | 61.1 |
| 65 | NGC 4235 | 9679 | Sa | 37.4 |
| 66 | UGC 11614 | 15682 | Sb | 105.0 |
| 67 | IC 5181 | 16757 | S0 | 24.1 |
| 68 | NGC 7232 | 16791 | S0-a | 23.1 |
| 69 | ESO 471-G024 | 17877 | S0-a | 113.0 |
| 70 | NGC 482 | 1009 | Sab | 85.0 |
| 71 | NGC 522 | 1102 | Sbc | 32.8 |
| 72 | NGC 585 | 1169 | Sa | 68.9 |
| 73 | NGC 653 | 1286 | Sab | 69.9 |
| 74 | NGC 684 | 1382 | Sb | 44.1 |
| 75 | NGC 1596 | 3625 | S0 | 20.5 |
| 76 | IC 2085 | 3680 | S0-a | 13.4 |
| 77 | NGC 2295 | 5413 | Sab | 26.9 |
| 78 | ESO 311-G012 | 6172 | S0-a | 18.2 |
| 79 | NGC 3203 | 7996 | S0-a | 37.5 |
| 80 | NGC 3404 | 8433 | SBab | 66.8 |
| 81 | NGC 5047 | 10588 | S0 | 88.7 |
| 82 | ESO 321-G010 | 9597 | Sa | 46.5 |
| 83 | ESO 416-G025 | 2246 | Sb | 65.0 |
| 84 | NGC 3390 | 8406 | Sb | 45.7 |
| 85 | IC 127 | 1149 | Sb | 23.1 |
| 86 | NGC 3628 | — | Sb | 16.2 |
| 87 | NGC 3717 | — | Sb | 28.2 |
| 88 | NGC 5965 | 12550 | Sb | 46.8 |
| 89 | NGC 4013 | 9412 | Sb | 14.5 |
| 90 | ESO 446-G018 | 11466 | Sb | 67.5 |
| 91 | ESO 512-G012 | 11898 | Sb | 49.5 |
| 92 | NGC 4710 | 10109 | S0-a | 19.6 |
| 93 | NGC 7814 | — | Sab | 9.5 |
| 94 | ESO 240-G011 | — | Sc | 35.7 |
| 95 | NGC 4565 | — | Sb | 20.7 |
| 96 | NGC 5746 | — | SABb | 26.4 |
| 97 | NGC 891 | — | Sb | 4.3 |
| 98 | NGC 5775 | 12067 | SBc | 25.7 |
| 99 | NGC 4217 | 9661 | Sb | 16.8 |
| 100 | NGC 5908 | — | Sb | 45.6 |
| 101 | NGC 4244 | — | Sc | 6.8 |
| 102 | NGC 4570 | 9935 | S0 | 28.1 |
| 103 | NGC 5907 | 12346 | Sc | 10.0 |
| 104 | NGC 3564 | — | S0 | 42.5 |
| 105 | NGC 4266 | 9707 | SBa | 25.6 |
| 106 | IC 4202 | 10456 | Sbc | 98.5 |
| 107 | NGC 4703 | 10103 | Sb | 64.5 |
| 108 | ESO 443-G042 | 10371 | Sb | 43.5 |
| 109 | NGC 5308 | 11118 | S0 | 29.1 |
| 110 | NGC 5365A | 11257 | SBb | 40.5 |
| 111 | IC 1048 | 11928 | Sb | 25.2 |
| 112 | UGC 243 | 293 | Sb | 66.6 |
| 113 | ESO 315-G020 | 7524 | Sb | 68.9 |
| 114 | NGC 669 | 1340 | Sab | 59.5 |
| 115 | NGC 973 | 2024 | Sb | 62.4 |
| 116 | IC 335 | 2973 | S0 | 20.7 |
| 117 | IC 1970 | 2982 | Sb | 15.9 |
| 118 | NGC 1380A | 2985 | S0 | 20.0 |
| 119 | ESO 362-G011 | 4306 | Sbc | 18.8 |
| 120 | NGC 1886 | 4383 | Sbc | 24.3 |

**Table 1.** continued.

| # | Galaxy | 2MFGC | Type | $D$ (Mpc) |
|---|---|---|---|---|
| | (1) | (2) | (3) | (4) |
| 121 | NGC 2310 | 5487 | S0 | 17.9 |
| 122 | NGC 2654 | 6926 | SBab | 19.8 |
| 123 | NGC 2862 | 7315 | SBbc | 58.9 |
| 124 | NGC 3126 | 7847 | Sb | 73.2 |
| 125 | NGC 3692 | 8974 | Sb | 28.3 |
| 126 | NGC 3957 | 9342 | S0-a | 27.1 |
| 127 | NGC 4417 | 9805 | S0 | 15.8 |
| 128 | NGC 1247 | 2619 | Sbc | 50.9 |
| 129 | NGC 5981 | 12588 | Sbc | 24.5 |
| 130 | NGC 4026 | 9425 | S0 | 15.3 |
| 131 | NGC 3501 | — | Sc | 20.0 |
| 132 | NGC 5023 | 10525 | Sc | 8.3 |
| 133 | NGC 360 | 761 | Sbc | 30.1 |
| 134 | UGC 1817 | 1825 | Scd | 47.2 |
| 135 | MCG-02-10-009 | 3079 | Sc | 27.7 |
| 136 | UGC 3326 | 4605 | Sc | 55.1 |
| 137 | UGC 3474 | 5237 | Sc | 49.1 |
| 138 | NGC 3044 | 7660 | SBc | 22.3 |
| 139 | NGC 3279 | 8207 | Sc | 23.7 |
| 140 | NGC 4222 | 9670 | Sc | 7.7 |
| 141 | ESO 533-G004 | 16767 | Sc | 31.2 |
| 142 | NGC 4330 | 9747 | Sc | 25.8 |
| 143 | ESO 564-G027 | 7159 | Sc | 33.8 |
| 144 | ESO 531-G022 | 16371 | Sbc | 42.1 |
| 145 | IC 4393 | 11612 | Sc | 40.5 |
| 146 | ESO 263-G015 | 7900 | Sc | 38.0 |
| 147 | NGC 4835A | 10246 | Sc | 49.3 |
| 148 | ESO 288-G025 | 16587 | Sbc | 30.7 |
| 149 | IC 2058 | 3483 | Scd | 18.6 |
| 150 | ESO 201-G022 | 3389 | Sc | 55.4 |
| 151 | IC 4871 | 15015 | SABc | 25.1 |
| 152 | IC 4484 | 11988 | Sc | 61.3 |
| 153 | ESO 340-G008 | 15435 | Sc | 36.1 |
| 154 | UGC 12533 | 17534 | Sb | 75.8 |
| 155 | ESO 509-G019 | 10818 | Sbc | 144.0 |
| 156 | ESO 506-G002 | 9712 | Sbc | 57.9 |
| 157 | NGC 4183 | 9620 | Sc | 15.8 |
| 158 | NGC 4517 | 9881 | Sc | 20.1 |
| 159 | NGC 2357 | 5811 | Sc | 33.0 |
| 160 | UGC 5173 | 7514 | Sb | 87.6 |
| 161 | NGC 100 | 282 | Sc | 6.7 |
| 162 | ESO 121-G006 | 4933 | Sc | 17.6 |
| 163 | NGC 2424 | 6083 | SBb | 47.3 |
| 164 | IC 2207 | 6207 | Sc | 66.7 |
| 165 | ESO 563-G014 | 6848 | SBcd | 27.1 |
| 166 | UGC 6012 | 8487 | Sbc | 88.8 |
| 167 | ESO 507-G007 | 10056 | Sbc | 75.2 |
| 168 | IC 3799 | 10098 | Scd | 54.4 |
| 169 | MCG-03-34-041 | 10613 | Sc | 40.2 |
| 170 | NGC 5073 | 10645 | SBc | 41.4 |
| 171 | IC 4351 | — | Sb | 39.8 |
| 172 | NGC 5529 | 11577 | Sc | 41.4 |
| 173 | NGC 5714 | 11872 | Sc | 32.1 |
| 174 | ESO 340-G026 | 15509 | Sc | 71.2 |
| 175 | UGCA 150 | 7144 | SABb | 29.3 |

Columns: (1) Name (the first in NED). (2) Number in 2MFGC (2MASS Flat Galaxy Catalog. (3) Morphological type taken from LEDA (Lyon/MeudonExtragalactic Database). (4) Angular-size distance ($H_0$ = 73 (km sec$^{-1}$)/Mpc, $\Omega_{\rm M}$ = 0.27, $\Omega_\Lambda$ = 0.73).